

Technical Report Documentation Page

1. Report No.		2. Government Accession No.		3. Recipient's Catalog No.	
4. Title and Subtitle Material Design and Structural Configuration of Link Slabs for ABC Applications				5. Report Date December 2018	
				6. Performing Organization Code	
7. Author(s) Behrouz Shafei, Peter Taylor, Brent Phares, Michael Dopko, Rizwan Karim, Shahin Hajilar, and Meysam Najimi				8. Performing Organization Report No.	
9. Performing Organization Name and Address Bridge Engineering Center Iowa State University 2711 South Loop Drive, Suite 4700 Ames, IA 50010-8664				10. Work Unit No. (TRAIS)	
				11. Contract or Grant No.	
12. Sponsoring Organization Name and Address Accelerated Bridge Construction U.S. Department of Transportation University Transportation Center Office of the Assistant Secretary for Florida International University Research and Technology 10555 W. Flagler Street, EC 3680 and Federal Highway Administration Miami, FL 33174 1200 New Jersey Avenue, SE Washington, DC 20590				13. Type of Report and Period Covered Final Report	
				14. Sponsoring Agency Code	
15. Supplementary Notes Visit www.intrans.iastate.edu for color pdfs of this and other research reports.					
16. Abstract Accelerated Bridge Construction (ABC) is now being widely used by the Departments of Transportation because of the reductions of traffic disruption, social cost, environmental impact, and lost time. ABC is also known to improve the work-zone safety, on-site constructability, and project completion time. One of the common techniques in ABC is using Prefabricated Bridge Elements and Systems (PBES). The bridge components are built outside of the construction area, transported on site, and then rapidly installed. Time lost due to concrete placement, curing in the construction zone, and formwork erection/removal is reduced. Another benefit to using prefabricated structural elements is the improved quality control. Damaging effects due to weather is minimized because elements are built in a controlled environment. Considering the advantages of PBES, a number of research projects have been conducted on the prefabrication and installation of the main structural elements of the bridges. However, there is a gap in the literature on how the long-term performance and durability concerns associated with the joints that connect already high-quality bridge elements may be addressed. One approach that has gained significant attention is to eliminate the joints through revised design strategies. While such strategies have been successfully developed for integral abutments used for ABC applications, no systematic study on removing the expansion joints between bridge girders has been found. To address this issue, the current research project investigates the use of a flexible link slab through a comprehensive set of experimental tests and numerical simulations. The outcome of this project is expected to provide the design guidelines and practical recommendations necessary to properly implement a link slab in the jointless bridges constructed with ABC and conventional techniques.					
17. Key Words accelerated bridge construction—link slabs—full-scale structural tests—fiber-reinforced concrete				18. Distribution Statement No restrictions.	
19. Security Classification (of this report) Unclassified.		20. Security Classification (of this page) Unclassified.		21. No. of Pages 151	22. Price NA

MATERIAL DESIGN AND STRUCTURAL CONFIGURATION OF LINK SLABS FOR ABC APPLICATIONS

**Final Report
December 2018**

Principal Investigator

Behrouz Shafei, Assistant Professor
Bridge Engineering Center, Iowa State University

Co-Principal Investigators

Peter Taylor, Director
National Concrete Pavement Technology Center, Iowa State University

Brent Phares, Director
Bridge Engineering Center, Iowa State University

Graduate Research Assistant(s)

Michael Dopko, Rizwan Karim, and Shahin Hajilar

Authors

Behrouz Shafei, Peter Taylor, Brent Phares,
Michael Dopko, Rizwan Karim, Shahin Hajilar, and Meysam Najimi

Sponsored by

Accelerated Bridge Construction University Transportation Center
U.S. Department of Transportation
Office of the Assistant Secretary for Research and Technology
and Iowa Department of Transportation

A report from
**Bridge Engineering Center
Institute for Transportation
Iowa State University**
2711 South Loop Drive, Suite 4700
Ames, IA 50010-8664
Phone: 515-294-8103 / Fax: 515-294-0467
www.intrans.iastate.edu

TABLE OF CONTENTS

ACKNOWLEDGMENTS	VIII
EXECUTIVE SUMMARY	IX
CHAPTER 1. INTRODUCTION	1
1.1. Research Significance	1
1.2. Scope and Objectives	2
CHAPTER 2. FLEXURAL PERFORMANCE EVALUATION OF FIBER REINFORCED CONCRETE FOR ABC APPLICATIONS	3
2.1. Fiber-Reinforced Concrete	3
2.2. Materials	4
2.3. Test Methods and Performance Parameters	5
2.4. Results and Discussion	8
2.5. Findings	11
CHAPTER 3. DIRECT TENSILE BEHAVIOR OF FIBER REINFORCED CONCRETE MATERIALS FOR DURABLE LINK SLABS	20
3.1. Direct Tensile Demand	20
3.2. Experimental Program	21
3.3. Findings	23
CHAPTER 4. FULL-SCALE STRUCTURAL TEST ON LINK SLAB	29
4.1. Experimental Setup	29
4.2. Testing Procedure	29
4.3. Results and Findings	30
CHAPTER 5. FEASIBILITY ASSESSMENT OF USE OF LINK SLABS IN A CASE STUDY BRIDGE	39
5.1. Link Slab in Practice	39
5.2. Existing Literature	39
5.3. Case-Study Bridge	42
5.4. Finite Element Models	42
5.5. Simulation Results	44
5.6. Findings	45
CHAPTER 6. CONCLUSIONS AND RECOMMENDATIONS	55
6.1. Summary	55
6.2. Significant Results and Findings	55
6.3. Future Work	56
REFERENCES	57

LIST OF FIGURES

FIGURE 1. Flexural test setup: main dimensions (top), and full configuration (bottom).....	14
FIGURE 2. A close view of fiber dispersion in broken beams made with 0.5%, 1.0%, and 1.5% (from left to right) of PP, PVA, and ARG fibers (from top to bottom).....	15
FIGURE 3. Cross section of broken PVA FRC beam with lumps of re-aggregated fibers.....	16
FIGURE 4. A close view of single (left) and double (right) crack pattern failure.	16
FIGURE 5. Load-deflection curves obtained from flexural tests on the specimens made with PP, PVA, and ARG fibers (1 in = 25.4 mm; 1 lb = 4.45 N).	17
FIGURE 6. Comparisons of the average with standard deviation of three flexural performance measures: (a) first peak strength, (b) $L/600$ deflection residual strength, and (c) $L/150$ deflection residual strength (1 psi = 0.0069 MPa).....	18
FIGURE 7. Comparisons of (a) toughness and (b) equivalent flexural strength ratio obtained for the three fibers tested in this study (1 in-lb = 0.113 Joules).	19
FIGURE 8. Dog-bone test specimen dimensions.	25
FIGURE 9. Direct tensile test set-up.	26
FIGURE 10. Load vs. average LVDT displacement a) up to 0.2 in displacement b) full displacement range.....	27
FIGURE 11. Rebar microstrain vs. average LVDT displacement.....	28
FIGURE 12. Load vs rebar microstrain up to rebar yield strain.....	28
FIGURE 13. A schematic view of the entire test setup.	33
FIGURE 14. Slab reinforcement.....	33
FIGURE 15. Reinforcement in the link slab.....	34
FIGURE 16. Instrumentation and debonding of the link slab portion.....	34
FIGURE 17. DCDT's and surface strain gauges.	35
FIGURE 18. Laboratory test setup.	35
FIGURE 19. Strain in the top surface gauge.	36
FIGURE 20. Strain in the rebar embedded in the link slab.	36
FIGURE 21. Maximum deflection at the center of the left span.	37
FIGURE 22. Beam profile under different support conditions.....	37
FIGURE 23. Crack pattern in the link slab at the ultimate stage.....	38
FIGURE 24. Crack patterns in the depth of the link slab at the ultimate stage.	38
FIGURE 25. Location (top) and schematic layout (bottom) of the case study bridge.	47
FIGURE 26. Full-scale 3D FE model of the case study bridge.....	48
FIGURE 27. An overview of the two sets of BSc used for the case study bridge.	49
FIGURE 28. Total stress at the pier base: DL + TL (left) and DL – TL (right).....	50
FIGURE 29. Exaggerated deformed shape of the bridge under +TL (top) and – TL (bottom). The deformation unit is inch.	50
FIGURE 30. Total stress under DL + TL at the pier base: Pier #1 (top) and Pier #2 (bottom).....	51
FIGURE 31. Bending moment in the piers for the four cases under +TL.....	52
FIGURE 32. Shear force in four piers for the four cases under +TL.	52
FIGURE 33. Axial force generated at the pier base for the four cases under +TL (top) and DL (bottom)	53
FIGURE 34. Exaggerated deformed shape of the bridge under DL + TL for four analysis cases: RwoLS and RwLS (top two), PwoLS and PwLS (bottom two).....	54

LIST OF TABLES

TABLE 1. Properties of three fiber types investigated in the current study.....	12
TABLE 2. Adjusted mix proportions after paste and HRWR additions.....	12
TABLE 3. Fresh properties of FRC mixtures.....	13
TABLE 4. Fiber properties.	24
TABLE 5. Mixture proportions.	24
TABLE 6. Properties of reinforcing bars.....	24
TABLE 7. Reinforcement details for the deck slab.....	32
TABLE 8. Reinforcement details for the link slab.	32
TABLE 9. Strains at the ultimate stage.	32

ACKNOWLEDGMENTS

This project was sponsored by the Accelerated Bridge Construction University Transportation Center (ABC-UTC at www.abc-utc.fiu.edu) at Florida International University (FIU), as the lead institution, and Iowa State University (ISU) as a partner institution, and the U.S. Department of Transportation (DOT) Office of the Assistant Secretary for Research and Technology.

The research team would like to extend a special appreciation to the ABC-UTC, and they would like to also thank the Iowa DOT, especially Mr. Ahmad Abu-Hawash, for providing the matching fund and technical support for this project.

The authors are grateful for the contributions of Owens Corning, ReforceTech, Forta, and Kuraray for their generous donation of fibers. The assistance of lab personnel, Bob Steffes and Jeremy McIntyre, as well as Doug Wood and Owen Steffens, is appreciated as well.

EXECUTIVE SUMMARY

Accelerated Bridge Construction (ABC) is now being widely used by the Departments of Transportation because of the reductions of traffic disruption, social cost, environmental impact, and lost time. ABC is also known to improve the work-zone safety, on-site constructability, and project completion time. One of the common techniques in ABC is using Prefabricated Bridge Elements and Systems (PBES). The bridge components are built outside of the construction area, transported on site, and then rapidly installed. Time lost due to concrete placement, curing in the construction zone, and formwork erection/removal is reduced. Another benefit to using prefabricated structural elements is the improved quality control. Damaging effects due to weather is minimized because elements are built in a controlled environment. Considering the advantages of PBES, a number of research projects have been conducted on the prefabrication and installation of the main structural elements of the bridges. However, there is a gap in the literature on how the long-term performance and durability concerns associated with the joints that connect already high-quality bridge elements may be addressed. One approach that has gained significant attention is to eliminate the joints through revised design strategies. While such strategies have been successfully developed for integral abutments used for ABC applications, no systematic study on removing the expansion joints between bridge girders has been found. To address this issue, the current research project investigates the use of a flexible link slab through a comprehensive set of experimental tests and numerical simulations. The outcome of this project is expected to provide the design guidelines and practical recommendations necessary to properly implement a link slab in the jointless bridges constructed with ABC and conventional techniques.

CHAPTER 1. INTRODUCTION

1.1. Research Significance

The bridge inventory in the United States is rapidly aging, with many of these structures nearing the end of their intended service life. When these deteriorating bridges need to be repaired or replaced, summation of the personal and economic loss across the country due to traffic closures will be astronomical. Transportation officials and bridge engineers have acknowledged this looming issue and developed a solution in the form of Accelerated Bridge Construction (ABC). ABC uses advanced scheduling and construction methods in order to minimize the time it takes to repair or replace a bridge structure, thereby minimizing traffic disruption and the associated economic and personal loss. Construction time can be reduced from months to weeks using ABC technology. Typical ABC construction practices utilize advanced construction materials, including cast-in-place concrete mixtures that rapidly gain strength or pre-cast concrete elements that are cast and adequately cured off-site then assembled to form the global structure in a rapid fashion.

The goal of ABC is not only to provide bridge designs and construction methods that result in speedy construction, but to produce finished bridges that are also durable and long lasting. This is to ensure that the solution is able to provide extended service life in order to avoid future repairs. One of the most problematic components to existing simple span bridges are expansion joints. Expansion joints exist over piers between simply supported spans of bridges and provide a gap for the bridge girder and deck system to rotate, expand and contract. Expansion joints can cause long term durability issues due to the ingress of corrosive materials through the gap they provide which prematurely deteriorates the underlying structure. Debris from the bridge deck can also accumulate in the expansion joint which restricts joint movement and causes damage. Due to these defaults, multiple expensive rehabilitation projects need to be performed on these expansion joints throughout the service life of the bridge. Expansion joints do not fit the second criteria previously described for ABC construction – expansion joints are not durable and long lasting.

Link slabs are a potential solution to the problems associated with expansion joints in bridge decks. Link slabs replace expansion joints over intermediate piers and create a continuous bridge deck system, while maintaining simply supported girder conditions under the deck. Link slabs eliminate the route for ingress of corrosive solutions, however they are subject to high moments and axial forces imposed by thermal and service loading of the supporting girders. Due to this demand, link slabs must be very durable and able to withstand high tensile loads while maintaining crack resistant properties to prevent ingress of corrosive materials to the reinforcement and underlying structure. Link slabs have been used as an effective solution by some state transportation agencies around the U.S., however their use is not widespread and use with ABC methodology is not well explored. The applications of link slabs for ABC include not only the timely retrofitting of existing simple span bridge expansion joints, but the use of link slabs with pre-cast deck and girder elements.

1.2. Scope and Objectives

The present report is intended to explore the use of link slabs in conjunction with ABC methodology. In order to address this research need, the current report will first address link slab materials related solutions. In order to achieve ABC solutions that are effective, the proposed method must be long lasting, fast and economically feasible. In the current report, these three criterion are investigated in a systematic fashion in order to produce sensible ABC link slab design recommendations.

The second chapter of this report presents the findings of an experimental study conducted on FRC beam specimens made with varying volumetric dosage rates of typical synthetic concrete fibers. The objective of the study is to compare the contributions of each fiber type to workability and performance under flexural induced tensile loads to determine the most effective fiber type for crack control applications. The findings of this study can be utilized to select an optimal fiber type and dosage rate for a cast-in-place link slab material in order to produce a durable, constructible and effective solution.

The third chapter further evaluates the performance of the ABC link slab material developed with the findings of chapter 2. Various mixtures are tested under uniaxial tension with steel and glass fiber reinforced polymer (GFRP) rebar embedded into the large dog-bone shaped test specimens. In order to evaluate the effectiveness of the fibers in the composite system, the material is tested with and without fiber. In addition, the material is compared against the performance of commercially available ultra-high performance concrete (UHPC) including steel fibers under the same testing conditions. The findings of this study contrast the compatibility of different classes of fiber reinforced cementitious materials with reinforcing materials of varying ductility and stiffness in order to evaluate their use in link slabs. Cracking behavior, rebar deformation behavior, and global deformation will be related in order to formulate design recommendations.

The fourth chapter of this report presents the results of an experimental full-scale test conducted on a half-depth link slab made with FRC in the laboratory. The main objective of this study is to explore the stresses developed in the link slab under different support conditions and investigate the effectiveness of fiber reinforced concrete (FRC) for use in link slabs. The conclusions of the study help in understanding the structural behavior of link slabs under the support conditions that represent real cases. The observations on crack initiation and propagation at ultimate loading demonstrate the ability of tension stiffening and small crack widths in FRC, and thus the suitability of use of FRC for link slabs in bridges.

The fifth chapter of the report provides a case study on a bridge with and without link slab investigated using 3D finite element models. The main objective of the study is to evaluate the feasibility of using link slabs in existing bridge structures. The study focused on the forces developed in the bridge pier and deck-girder system. The study findings help with realizing that as the bearing pad in bridges age, they start to behave like a pin rather than a roller and cause additional stresses in the deck and girder structure. The study supports the use of link slabs for rehabilitation purposes as the link slab will result in minimal stresses when pinned connections are used.

CHAPTER 2. FLEXURAL PERFORMANCE EVALUATION OF FIBER REINFORCED CONCRETE FOR ABC APPLICATIONS

2.1. Fiber-Reinforced Concrete

Formation and propagation of cracks in concrete is a complex process, which starts with the development of micro cracks under the tensile stresses that exceed the concrete's tensile strength. Micro cracks then grow together and form macro cracks, which can propagate under tensile stresses until the crack becomes unstable and fracture occurs. In order to control the cracks and avoid a brittle failure mode, continuous reinforcement in the form of rebar or welded wire mesh is conventionally placed in the zones of the concrete where a tensile stress is expected. To further help avoid brittle failure and control crack formation and propagation in concrete, relatively short fibers can be dispersed randomly throughout the concrete matrix during the mixing process. In certain applications, such fibers can not only reduce the required thickness, but potentially eliminate the need for continuous reinforcement, especially in concrete slabs.

The size, type, and other physical characteristics of fibers used in concrete are known to greatly affect the mixture properties in both fresh and hardened states. One common approach to categorize concrete fibers is by their size. In general, for conventional fiber reinforced concrete (FRC), small "micro" fibers are used to prevent early-age cracking and increase the pre-crack performance of the matrix by arresting micro cracks, as they form. On the other hand, relatively large "macro" fibers are included to provide load carrying capacity and toughness after a crack has formed (i.e., residual strength), as well as to control the propagation of cracks that have grown past the micro stage (Banthia and Soleimani (2005)). Another approach to categorize concrete fibers is by the material they are made from. Steel fibers have shown many benefits to the mechanical properties of FRC (Thomas and Ramaswamy (2007)), but they face corrosion issues in the presence of harsh environmental conditions that civil structures are frequently exposed to. Natural fibers in concrete have received a significant attention lately, however, most of them face certain limitations, such as high water absorption and lack of long-term stability in the highly alkaline concrete environment (Bentur and Mindes (2006)). The apparent limitations of steel and natural fibers in concrete have resulted in a growing interest in synthetic fibers that can avoid corrosion and strength degradation, even after a long period of time. Carbon, aramid, polyethylene, nylon, polypropylene, polyolefin, acrylic, polyvinyl alcohol, alkali resistant glass, and more recently basalt are among synthetic fibers that have been explored for use as concrete fibers for a variety of applications (Zheng and Feldman (1995), Alani and Bucket (2013), Patnaik et al. (2013), Dopko et al. (2011)).

In the situations that the hardened composite is expected to exhibit high post-crack (residual) strength and toughness, as well as avoid deterioration from chemical instability or corrosion, macro synthetic fibers are a sensible addition to the mixture. There is an abundance of literature that highlights the flexural and/or tensile performance of a single synthetic fiber type (Mohod (2005), Patnaik et al. (2013), Hamoush et al. (2010)) or multiple fiber types mixed together (Buratti et al. (2011), Shafiq et al. (2016)). However, in order to obtain a proper comparison between synthetic fiber types, the fibers must share characteristics that make them suitable for improving the performance metrics of interest, including post-crack strength and toughness. Although some studies have compared different macro synthetic fiber types (e.g., Roque et al.

(2009), Fraternali et al. (2011)), there is a need for an in-depth study pertaining to the comparisons of workability, residual flexural strength, and toughness provided by different commercially available macro-synthetic fibers that have potential to provide high residual strength and toughness in concrete. To address this research gap, the current study investigates three types of synthetic macrofibers dispersed in a consistent concrete matrix. Static and dynamic fresh properties are monitored using the vibrating Kelly ball (VKelly) test, and hardened properties are evaluated using the flexural testing method in accordance with the ASTM C1609 Standard. The fibers of choice include polypropylene (PP), polyvinyl alcohol (PVA), and alkali-resistant glass (ARG) macrofibers with reasonably similar aspect ratios. These three fiber types are selected based on their availability in the current concrete market and potential to provide high post-crack strength and toughness. The findings of this study provide insight into the capabilities and limitations of different types of market available synthetic macrofibers in the fresh and hardened state, further advancing the state of practical FRC knowledge through a comparative analysis.

2.2. Materials

2.2.1. Fibers

Three types of macro-synthetic concrete fibers with comparable aspect ratios (i.e., PP, PVA, and ARG) are chosen to assess their flexural reinforcing potential as per the ASTM C1609 Standard. PP fibers are one of the most common types of synthetic concrete fibers due to their relatively low cost, chemical stability in alkaline environment, and availability. Limitations of PP include low modulus of elasticity and poor bond with the concrete matrix. Bond properties of PP fibers can be enhanced by manufacturing the fibers with a twisted shape or texturing the fiber surface. Fibrillated micro PP fibers are a common concrete micro fiber mostly used to control cracking induced by plastic shrinkage in concrete applications with a large exposed surface (Banthia and Gupta (2006)). The macro PP fibers used in this study are a blend composed mostly of twisted bundle monofilament macrofibers, as well as a low volume of fibrillated strands.

Polyvinyl alcohol (PVA) fibers are gaining popularity in the concrete market for several applications. PVA was initially developed to replace asbestos in making fiber cement using the hatcheck process (Studinka (1989)). This type of fiber is very stable in the chemistry of the concrete environment, has a relatively high modulus of elasticity, and is reported to have the unique ability to chemically bond with the concrete matrix (Betterman et al. (1995)). Due to the superior bond properties of PVA, the fibers used in concrete are typically monofilament with no surface deformations. Micro PVA fibers are a key ingredient in Engineered Cementitious Composite (ECC), which utilizes a high volume of PVA fibers and fly ash to form a hardened mortar that is capable of up to 5% tensile strain due to multiple, closely-spaced micro cracks, which provide a pseudo strain hardening behavior under tensile strains (Li (2008)). The PVA fibers used in this study are monofilament, straight, and have no surface deformations.

ARG fibers are relatively new to the concrete market and are made from extruding melted volcanic rock into filaments and forming strands of the desired size to be cut to the desired length (Mohammadi (2016)). ARG fibers have a relatively high modulus of elasticity, but this depends on the type of ARG fiber under consideration. Chopped ARG fibers made from this process tend to have a small diameter and high aspect ratio, categorizing them as a microfiber.

They are also known to experience strength degradation in the alkaline environment of the concrete, much like glass fibers (Wu et al. (2015)), limiting their applications to early-age plastic shrinkage crack control. More recently, a ARG macrofiber has been developed by impregnating multiple ARG fiber filaments in a highly alkali proof resin. The resin coating also helps improve the fibers ability to bond with the concrete matrix. The fibers have a subtle twisted shape along their length to increase mechanical bond to the concrete matrix. This type of fiber has shown high post-crack load bearing capacity and toughness in FRC. They are also reported to disperse well in concrete due to their density being similar to that of the concrete matrix (Patnaik et al. (2014)). The ARG fibers used in this study are monofilament, made with multiple resin impregnated strands and have a subtle twist along their length. Table 1 lists the main properties of the three fiber types used in the current study. Since 3/8 inch maximum aggregate size is used, fiber length is decided to be at least 3/4 inch to increase the fiber's reinforcing potential around the largest aggregate particles.

2.2.2. Concrete Matrix Composition

The base concrete mixture proportions are chosen to favor workability and reinforcing potential of the selected fibers. Type I/II Portland cement is used with 30% cement replacement with Class F fly ash to improve workability. 3/8 inch (9.5 mm) maximum size crushed limestone is utilized for coarse aggregate and river sand is used for fine aggregate. 3/8 inch maximum size aggregate is chosen to maximize the volume within the matrix that fibers could exist without their position and orientation being restricted. This also improves the workability of FRC mixes, as limiting the maximum aggregate size increases the volume space available for the fibers when the mixture is in the fluid state (Johnston (2014)).

Water-to-cementitious materials ratio is held constant for all mixtures at 0.38. Since each of the three fibers tested has a different surface area per unit volume, and three different volumes are tested per fiber type, different amounts of polycarboxylate high-range water reducer (HRWR) and cement paste are added to each base mixture during the mixing process in order to maintain satisfactory fresh properties for adequate consolidation under external vibration. Paste is prepared with the same water to cementitious materials ratio as the base mix design in order to avoid affecting the strength of the hardened composite. The paste additions are deemed necessary to coat the extra surface area of the fibers and provide adequate fresh properties. Table 2 summarizes mixture proportions of each mixture after the paste and HRWR additions. Cross sections of the broken beams for each mixture show the amount of fibers present and the dispersion of the fibers throughout the concrete matrix (Figure 2).

2.3. Test Methods and Performance Parameters

2.3.1. Test Methods

The VKelly test is employed to evaluate the fresh properties of the fiber mixtures designed for the current study. This test measures two parameters: (1) VKelly slump, which is a parameter indicating the fresh concrete mixture's initial yield stress and is calculated by doubling the Kelly ball penetration into the fresh concrete under its own weight; and (2) VKelly index, which is expected to report how well the mixture responds to vibration for consolidation. The VKelly

index is found by timing the Kelly ball's penetration depth into the fresh concrete under controlled external vibration at six-second intervals. This source of data is then used to plot the penetration depth versus time^{0.5}, the slope of which is taken as the VKelly index. To calculate the VKelly index of each mixture, three test trials are performed and obtained values are averaged. The VKelly test was originally developed for slip-form paving applications, for which a VKelly index of 0.6-1.2 in/s^{0.5} (15-30 mm/s^{0.5}) was deemed suitable. Further details of the VKelly test can be found in Taylor et al. (2015).

The ASTM C1609 Standard (I7) is used to evaluate the flexural performance of the FRC mixtures. Following this standard, third point bending tests are carried out using a 400 k (1780 kN) capacity Instron universal testing machine with external data acquisition system connected to two Linear Variable Differential Transformers (LVDTs). The support span length on the bottom of the beams is set to 12 inches (305 mm), while two point loads are applied to the top of the beam spaced 4 inches (100 mm) apart, as well as placed symmetrically 4 inches (100 mm) inside of the bottom supports (Figure 1a). The supports and top load applicators are made from oval shaped dowel bars to facilitate free rotation at the supports. Because the supports of the testing apparatus are restrained against translational movement, some lateral friction forces can be generated between the specimen and the bottom supports as the deflection increases during the test. This may cause some pseudo deflection hardening behavior, especially at high deflection values. However, since all specimens are tested under the same condition, consistent comparisons are drawn between different fiber types and dosages based on the data collected. Aluminum tabs are glued to the specimen at the mid-span on both sides of the beam, while magnetic stands are used to hold LVDTs under each tab in order to measure the mid-span deflection (Figure 1b). The average deflection found using values from both sides of the beam are used to calculate the flexural performance parameters. Following the ASTM C1609 Standard, the mechanical load is applied in a displacement-controlled manner at a loading rate of 0.003 inches (0.075 mm) per minute up to a deflection of $L/900$, where L is the support span length. After this deflection is reached, the loading rate is increased to 0.005 inches (0.127 mm) per minute for the remainder of the test. In the current study, three beams sized 4×4×14 inches (100×100×350 mm) are cast for each fiber type and dosage, making a total of 27 specimens. The beam molds are oiled prior to casting and the fresh concrete is consolidated using a vibrating table. Preferential alignment of the fibers during casting is avoided to the extent possible. The specimens are demolded after 24 hours and allowed to cure at 73 °F (23 °C) and 100% relative humidity. All the beams are tested at 7 days of age.

2.3.2. Flexural Performance Parameters

According to the ASTM C1609 Standard, a set of measures can be formulated to compare the performance of various specimens based on the load versus deflection curves obtained from the test. The strength in the specimens at any deflection value is calculated using the specimen dimensions as well as the load resisted at the corresponding deflection by the following equation (Eq. 1):

$$f = \frac{PL}{bd^2} \quad (1)$$

where:

f = strength (psi, MPa)

P = load (lbf, N)

L = span length (in, mm) - 12 inches (305 mm) for this study

b = specimen width (in, mm) - 4 inches (100 mm) for this study

d = specimen depth (in, mm) - 4 inches (100 mm) for this study

Eq. 1 is employed to find the modulus of rupture, which can be considered as a measure of the beam's flexural strength. The modulus of rupture is very nearly the same as the first peak flexural strength, f_1 , associated with the load immediately prior to crack formation, P_1 . At deflections larger than that corresponding to the first peak load, the residual load carrying capacity is provided by the fibers in the mixture. Residual load parameters of P_{600} and P_{150} for deflections of $L/600$ and $L/150$, respectively, are used to compute residual strength parameters, f_{600} and f_{150} , using Eq. 1, with the load at the corresponding deflections. Residual strength refers to the ability of the FRC specimen to sustain load after cracking has occurred.

In addition, toughness up to a net deflection of $L/150$ (T_{150}) is obtained by calculating the area under the load-deflection curve up to the corresponding deflection (i.e., 0.08 inches (2 mm) for the beam dimensions used in this study). Toughness, which is defined as the energy absorbed by the specimen throughout the loading process, can be considered as an important parameter for indicating the flexural performance of FRC mixtures. This is primarily because it quantifies the post-crack load carrying capacity of the specimen through the entire specified range of deflections.

Finally, the equivalent flexural strength ratio is computed using the following equation:

$$R_{T150} = \frac{150T_{150}}{f_1bd^2} * 100\% \quad (2)$$

where:

R_{T150} = equivalent flexural strength ratio (%)

f_1 = first peak strength (psi, MPa)

T_{150} = Toughness up to $L/150$ deflection (in-lb, Joules)

b = specimen width (in, mm) - 4 inches (100 mm) for this study

d = specimen depth (in, mm) - 4 inches (100 mm) for this study

The equivalent flexural strength ratio is a parameter that relates the first peak flexural strength to the toughness of the composite. A low first peak strength and high toughness would result in a high R_{T150} value, while a high first peak strength and low toughness would result in a low R_{T150} value. Since this study utilizes the same concrete matrix for all mixtures, it is expected that R_{T150} values follow the same trend as the toughness values for each mixture. Using the performance parameters from the ASTM C1609 Standard, a three-specimen average and standard deviation are calculated for the performance parameters of interest. The analysis of such parameters along with the original load-deflection curves provides an in-depth insight on the promise of each fiber type and volume percentage.

2.4. Results and Discussion

2.4.1. Fresh Properties

During the process of mixing and casting the FRC specimens, each fiber type is found to affect the fresh properties of the mixture differently. Table 3 shows the percentage of paste and HRWR dosage added to each mixture along with the corresponding VKelly slump and index. Results show that the PP fibers mix well at 0.5% and 1.0% volumes with a relatively low effect on workability, which can be compensated for by small additions of HRWR. At the 1.5% volume of PP fibers, however, the mixture becomes considerably stiff with an insufficient response to vibration, as reflected in the relatively low VKelly index of $0.13 \text{ in/s}^{0.5}$ ($3.3 \text{ mm/s}^{0.5}$), even after the addition of paste and HRWR.

The PVA fibers show certain limitations in the fresh state. At 0.5% volume, they mix very well with adequate dispersion and workability. However, the response to vibration is so high that the ball moves through the concrete and no reading can be taken past 6 seconds. This is the reason for the absence of a reported value for the VKelly index of PVA0.5 mixture in Table 3. For the 1.0% and 1.5% volume PVA mixtures, clumping of the fibers becomes an issue, as once the volume percentage of fibers exceeds a certain limit, the fibers come together and form 1 to 2 inch diameter clumps that contain only sand, fiber, and paste (Figure 3). Considering that continued mixing would not disperse the clumps, the specimens are cast and consolidated with the existing clumps. Although fiber dispersion admixtures like methylcellulose, latex, and acrylic are reported to be effective (28), it was decided to not utilize these admixtures because they were not needed for PP and ARG mixtures, in addition to their lack of practicality in full-scale projects. ARG fibers demonstrate the smallest effect on the fresh properties of the mixture, which is expected due to their relatively low aspect ratio, as well as the specific gravity that is closest to that of the concrete matrix. The ARG fiber mixtures respond well to vibration, as can be inferred from their comparatively high VKelly indices. The VKelly index of the mixtures tested in this study are all below $0.6\text{-}1.2 \text{ in/s}^{0.5}$ ($15\text{-}30 \text{ mm/s}^{0.5}$), which is the VKelly index recommended for slip-form paving. This indicates that fiber addition has a strong effect on the fresh properties. While further research is needed to determine the optimal VKelly parameters for FRC mixtures, the values of VKelly index reported in this study can be effectively used for capturing the relations between fiber types, dosages and corresponding fresh properties.

2.4.2. Flexural Test Results

The beams made with the fiber types and dosages considered in the current study all show a deflection hardening behavior, immediately after the formation of the first crack. The first crack is characterized by the first sharp drop in the load-deflection curve, and a positive slope immediately following this drop indicates the deflection hardening behavior. For the specimens containing PVA fibers, this initial post-crack deflection hardening response is followed by a deflection softening behavior. One of the PVA0.5 beams did not have a completed data set because the load dropped past 20% of the initial value and the safety stop was triggered on the testing machine. The safety stop was adjusted to a lower value for subsequent tests. One of the

B1.5 specimens also did not have a completed data set because a crack formed directly under the portion of the beam where the aluminum tab was glued and the tab became disconnected. All volumes tested for PP and ARG show a continued deflection hardening behavior after the formation of the first crack. It is interesting to note the presence of a second sudden drop in some of the load-deflection curves, which is an indicator of a second crack forming in the specimen. This can be noticed for some of the B1.0 and B1.5 specimens, as well as one of the PP1.5 specimens. The presence of multiple cracks in the B1.0, B1.5, and PP1.5 specimens demonstrates the fiber's role to sufficiently transfer load across the crack, helping develop the full strength of the matrix. All other mixes listed in Table 3 are found to fail by a single crack that continues to propagate. Figure 4 shows the failed specimens with single and double cracking patterns for comparison. The load versus average mid-span deflection curves obtained for all 27 beams are shown in Figure 5.

The average and standard deviation of five performance parameters introduced by the ASTM C1609 Standard are extracted from load-deflection curves. Figure 6a contains the comparison of the three specimen average first peak strength, which is a measure of the composite flexural strength prior to cracking. It can be seen that for PP and ARG fibers, the first peak strength increases with the increase in fiber dosage. For PP fibers, this increase is small (close to 2%) when comparing the PP0.5 and PP1.0 specimens. However, the increase is found to approach 8% when the PP1.5 specimens are tested. For ARG fiber specimens, a larger increase (14.5%) in the first peak strength is recorded between the B0.5 and B1.0 specimens, while the increase becomes less significant (1.5%) when the B1.5 specimens are tested.

A 5.2% average decrease in the first peak strength occurred between the PVA0.5 and PVA1.0 specimens, but a 10.6% average increase occurred between the PVA1.0 and PVA1.5 specimens. The inconsistencies in the PVA fiber mixtures can be attributed to the lack of uniform dispersion present in the PVA1.0 and PVA1.5 mixtures, as the fiber clumps may have created weak spots in the beam. For the 0.5% fiber volume mixtures, PVA specimens show the highest first peak strength followed by PP and finally ARG. This trend is reversed for the 1.0% volume mixtures and continues for the 1.5% volume mixtures. Due to high standard deviations in the PP0.5, B0.5, PP1.5 and B1.5 data, it is uncertain as to which fiber provides a larger first peak strength. However, it can be generalized that increasing volumes of both PP and ARG macrofibers can slightly increase the first peak strength of the beams in the range of fiber volumes tested. Figures 6b and 6c represent the three specimen average and standard deviation for $L/600$ and $L/150$ residual strength for each mixture, respectively. It is clear that for all three fibers tested, increasing the fiber volume increases the residual strength. ARG specimens consistently provide the highest $L/600$ residual strength, while PP specimens show the lowest for 0.5% volume and PVA specimens show the lowest for 1.5% volume. The increase in the $L/600$ residual strength with increasing fiber volume is more pronounced for PP fiber specimens than for PVA fiber specimens. Large increases occurred in the $L/600$ residual strength with increasing PP and ARG fiber content, especially between the 0.5% and 1.0% fiber volumes. The PP1.0 specimen experiences a 148.4% increase over PP0.5, while the B1.0 specimen witnesses a 194.1% increase over B0.5. These increases become less pronounced with the increase of dosage to 1.5% for all the fibers, especially for ARG (4.0%). However, the increases still remain significant for PP1.5 (66.0%). The PVA specimens show a more linear increase in the $L/600$ residual strength across all three fiber volumes tested, but the increase is still over 20% higher between PVA0.5 and

PVA1.0 than between PVA1.0 and PVA1.5. The $L/150$ residual strengths shown in Figure 6c clearly indicate improvements with increasing fiber volumes for all three fibers tested, but the B1.0 mixture is found exceptionally high and PVA1.0 is found relatively low for the $L/150$ residual strength. PVA fiber mixtures also consistently show the lowest $L/150$ residual strengths, due to deflection softening behavior at higher deflections for all fiber volumes, while ARG fiber mixtures consistently show the highest $L/150$ residual strengths, due to the fibers ability to sustain loads at larger deflections.

Toughness is calculated as the area under the load-deflection curve up to $L/150$ deflection, as per the ASTM C1609 Standard. Figure 7a shows the three specimen average toughness with standard deviations included. For all the fibers tested, the toughness increases with increasing fiber volume percentage. The toughness of PP and PVA fiber mixtures show a linear increase with increasing fiber volume. ARG fiber mixtures, however, show a much larger increase in toughness from B0.5 to B1.0 (143.1%) compared to B1.0 to B1.5 (7.6%). PVA and ARG fiber mixtures consistently provide the lowest and highest toughness values, respectively. The equivalent flexural strength ratio of three specimen averages and standard deviations are shown in Figure 7b. The equivalent flexural strength ratios follow the same trend as toughness.

The post-crack performance parameters, including f_{600} , f_{150} , T_{150} , and R_{T150} demonstrate a consistent increase with increasing fiber volume for all the three fibers tested. PP results indicate linear increases with fiber volume for all the four post-crack parameters investigated. B1.0 samples are found to generate exceptional results compared to PVA1.0 and PP1.0 specimens. B1.0 results are also well above the linear trend between B0.5 and B1.5. The results indicate small benefit for flexural performance by increasing the ARG fiber percentage from 1.0% to 1.5% for the mix design used in this study. PVA fiber mixtures generally follow a linear increasing trend for post-crack parameters, despite the lack of consistent dispersion and difficulties encountered while mixing the fibers.

The fact that the fiber with the largest cross section and lowest aspect ratio shows the best flexural results in this study is counterintuitive, given that a higher aspect ratio and smaller diameter result in more surface area per volume of fibers being in contact with the concrete matrix. PP fibers have the highest aspect ratio and similar length to the ARG fibers, but did not perform as well as the ARG fibers, meaning that the ability of the ARG fibers to form a bond with the concrete matrix is superior to that of the PP fibers. The shorter PVA fibers have the second highest aspect ratio, but are about half as long as the PP and ARG fibers. This means that there are more PVA fibers per unit volume of concrete, but the fibers have less surface area available per fiber to bond with the concrete and develop the strength of the fiber cross section. Initially, the shorter PVA fibers were selected because of the reported ability to form a strong bond with concrete, but the results indicate that a longer PVA fiber may have been more effective in providing flexural residual strength and toughness. For all the three types of fiber, the failure mechanism is characterized by the fibers pulling out from the concrete matrix, rather than rupturing. This indicates that the limiting factor contributing to flexural and tensile performance is the bond strength between the fiber and the concrete matrix. A higher strength concrete matrix may have been able to develop more of the fiber strength and increase toughness. However, for the FRC mixture tested in this study, the obtained results indicate that

larger fibers with superior ability to resist pull-out from the concrete matrix are most effective to increase post-crack flexural properties.

2.5. Findings

This research effort focused on comparing the flexural performance of FRC made with three synthetic macrofibers with comparable aspect ratios (i.e., PP, PVA, and ARG fibers), dispersed at volume percentages of 0.5%, 1.0%, and 1.5%. The results of this work showed that the VKelly test qualifies as a suitable test for fresh properties of FRC, as it can capture static and dynamic responses, which are particularly important for fiber mixtures.

The results of the investigation of flexural performance of the tested FRC beams indicate that:

- Increasing fiber volumes for PP and ARG macrofibers slightly increase the first peak strength of the composite, but this trend was less pronounced and cannot be concluded based on the results of this study for the PVA macrofibers tested, likely due to weak spots in the cross section as a result of clumping during mixing.
- Increasing the fiber volume between 0.5% and 1.5% resulted in increased post-crack performance parameters of residual strength, toughness, and equivalent flexural strength ratio for the three fibers tested.
- ARG fibers consistently produced the highest residual strength and toughness values of the three fibers tested, with a more pronounced advantage for the 1.0% volume ARG fiber mixture. Small increases in all flexural parameters were noticed between the B1.0 and B1.5 mixtures for the concrete matrix used in this study. ARG fibers had the smallest effect on the fresh properties of the concrete at each volume tested.
- PVA fibers consistently produced the lowest toughness values for the three volume percentages tested. When PVA fiber volumes were increased to 1.0% or more, the fibers tend to re-aggregate and form clumps with the sand and paste, creating a non-homogenous mixture that has apparent effects on the composite pre-crack flexural performance, but less of an effect on the composite post-crack flexural performance.
- PP fibers showed the most consistent increases in post-crack flexural properties when fiber volumes were increased. Although the PP toughness and residual strengths were lower than those of ARG at all volumes, the PP0.5 versus B0.5 and PP1.5 versus B1.5 mixtures showed comparable flexural performance results. PP fibers mixed well at 0.5% and 1.0% volume, but the PP1.5 mixture had low vibrational response and would require a high HRWR dosage to achieve consolidation during large-scale placements, especially if rebar is present.
- A higher aspect ratio does not necessarily translate to higher flexural performance for the fibers tested in the current study. ARG fibers had the lowest aspect ratio, yet showed the highest flexural performance, likely due to the ability of the resin coating on the fibers to form a strong bond with the concrete.

TABLE 1. Properties of three fiber types investigated in the current study.

Fiber Type	PP	PVA	ARG
Diameter (inch (mm))	0.013 (0.34)	0.008 (0.2)	0.026 (0.65)
Length (inch (mm))	1.50 (38)	0.71 (18)	1.69 (43)
Aspect Ratio	112	90	66
Tensile Strength (ksi (GPa))	90 (0.62)	145 (1.00)	157 (1.08)
E. Modulus (ksi (GPa))	690 (4.7)	3920 (27)	6382 (44)
Specific Gravity	0.9	1.3	2.1

TABLE 2. Adjusted mix proportions after paste and HRWR additions.

Mix ID	Cementitious Materials (lb/cy (kg/m³))			Aggregates (lb/cy (kg/m³))		Water (lb/cy (kg/m³))	HRWR (oz/cwt)	Fiber Volume (%)
	Type I/II Cement	Class F Fly Ash	Total	Coarse	Fine			
Base Mix	593 (352)	254 (151)	847 (503)	1534 (910)	1257 (745)	322 (191)	0.0	0.0
PP0.5	593 (352)	254 (151)	847 (503)	1533 (909)	1256 (744)	322 (191)	0.6	0.5
PP1.0	599 (355)	257 (152)	856 (507)	1511 (896)	1239 (735)	325 (193)	1.8	1.0
PP1.5	607 (360)	260 (154)	867 (514)	1474 (874)	1208 (716)	330 (196)	3.1	1.5
PVA0.5	610 (362)	261 (155)	871 (517)	1505 (892)	1234 (732)	331 (196)	2.9	0.5
PVA1.0	636 (377)	272 (161)	908 (538)	1455 (863)	1193 (707)	346 (205)	2.8	1.0
PVA1.5	664 (394)	284 (168)	948 (562)	1397 (828)	1144 (678)	361 (214)	6.3	1.5
B0.5	593 (352)	254 (151)	847 (503)	1533 (909)	1256 (745)	322 (191)	1.0	0.5
B1.0	589 (349)	252 (149)	841 (498)	1525 (904)	1250 (741)	320 (190)	2.6	1.0
B1.5	594 (352)	255 (151)	849 (503)	1506 (893)	1234 (732)	333 (197)	2.6	1.5

TABLE 3. Fresh properties of FRC mixtures.

Mix ID	% Paste Added	HRWR (oz/cwt)	VKelly Slump		VKelly Index	
			Average (in (mm))	COV (%)	Average (inch/s ^{0.5} (mm/s ^{0.5}))	COV (%)
PP0.5	0.0	0.6	1.5 (38)	6.4	0.47 (11.9)	5.8
PP1.0	2.5	1.8	1.3 (33)	7.1	0.33 (8.4)	3.5
PP1.5	6.7	3.1	1.0 (25)	10.9	0.13 (3.3)	12.6
PVA0.5	4.9	2.9	2.6 (66)	15.4	N/A	N/A
PVA1.0	13.0	2.8	1.3 (33)	7.4	0.25 (6.4)	9.6
PVA1.5	23.1	6.3	2.0 (51)	8.2	0.19 (4.8)	12.6
B0.5	0.0	1.0	2.3 (58)	4.2	0.60 (15.5)	3.0
B1.0	0.0	2.6	1.9 (48)	13.4	0.43 (10.9)	3.1
B1.5	2.0	2.6	1.3 (33)	7.4	0.30 (7.6)	5.4

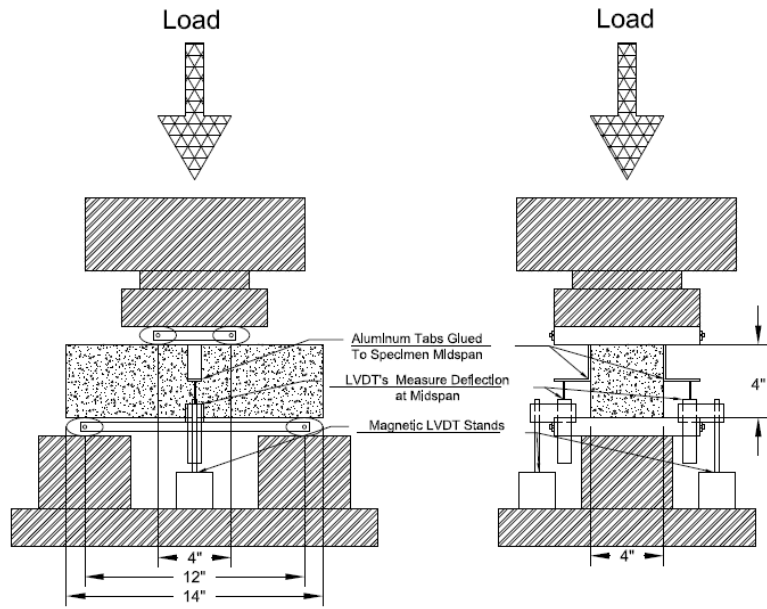


FIGURE 1. Flexural test setup: main dimensions (top), and full configuration (bottom).

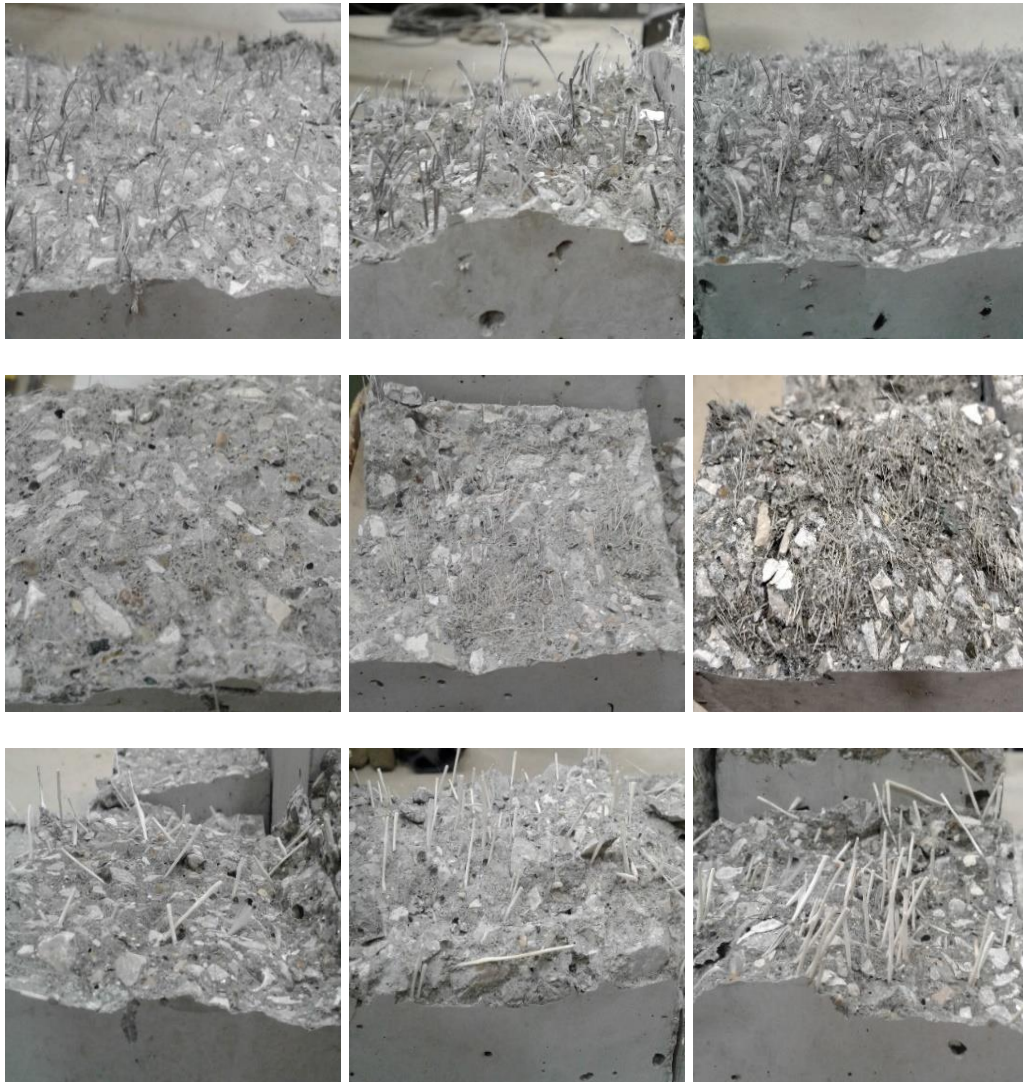


FIGURE 2. A close view of fiber dispersion in broken beams made with 0.5%, 1.0%, and 1.5% (from left to right) of PP, PVA, and ARG fibers (from top to bottom).

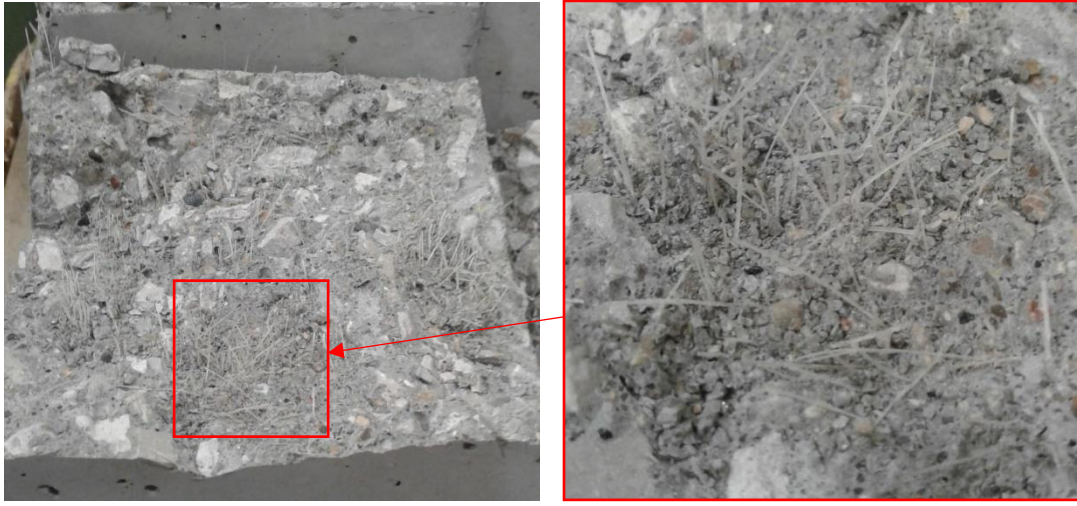


FIGURE 3. Cross section of broken PVA FRC beam with lumps of re-aggregated fibers.



FIGURE 4. A close view of single (left) and double (right) crack pattern failure.

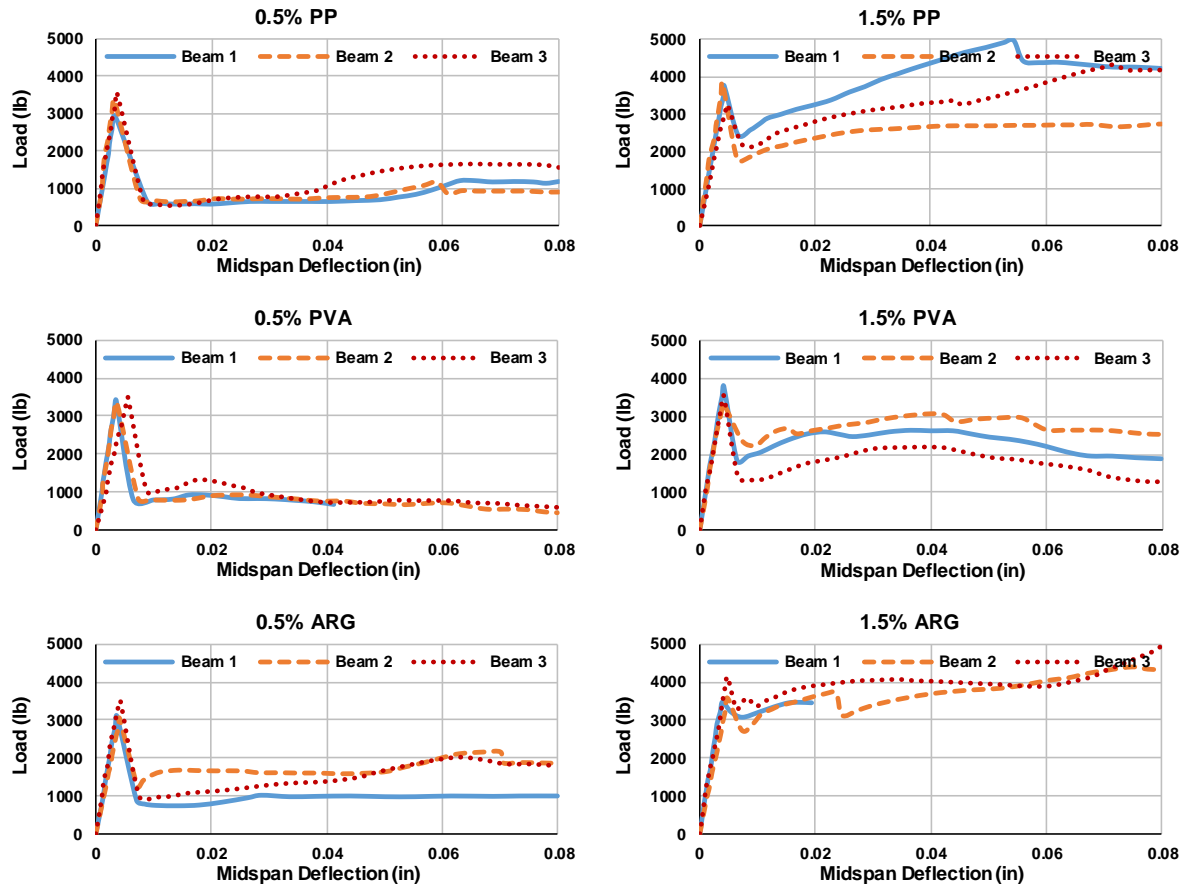


FIGURE 5. Load-deflection curves obtained from flexural tests on the specimens made with PP, PVA, and ARG fibers (1 in = 25.4 mm; 1 lb = 4.45 N).

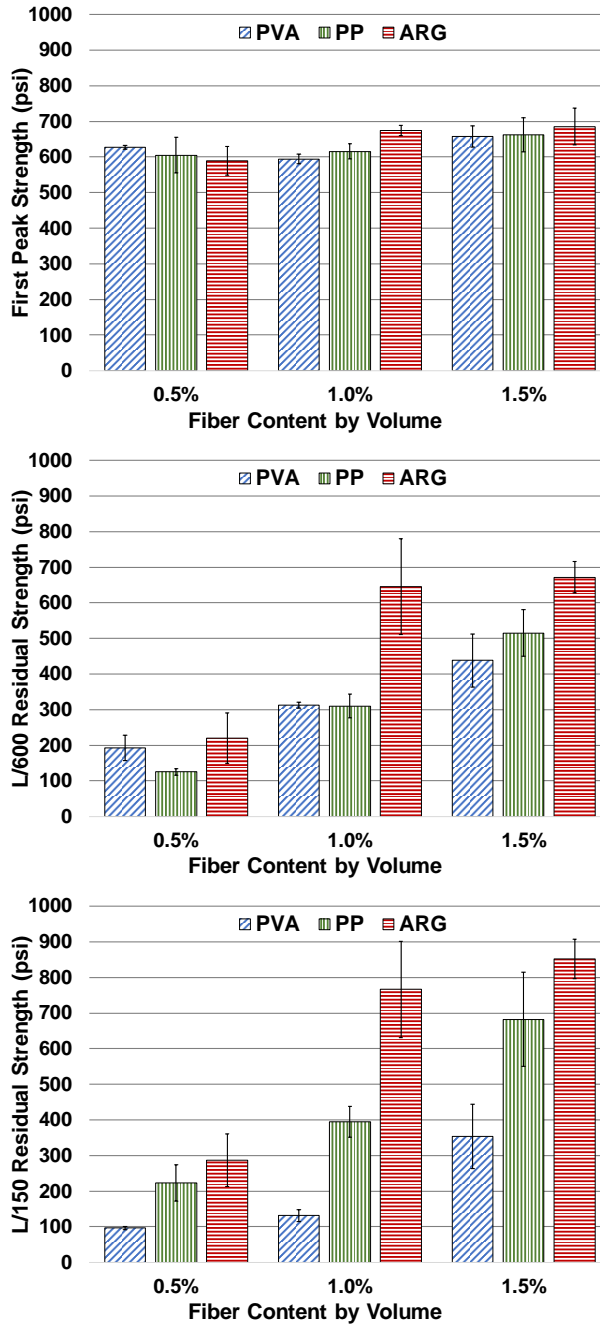


FIGURE 6. Comparisons of the average with standard deviation of three flexural performance measures: (a) first peak strength, (b) *L*/600 deflection residual strength, and (c) *L*/150 deflection residual strength (1 psi = 0.0069 MPa).

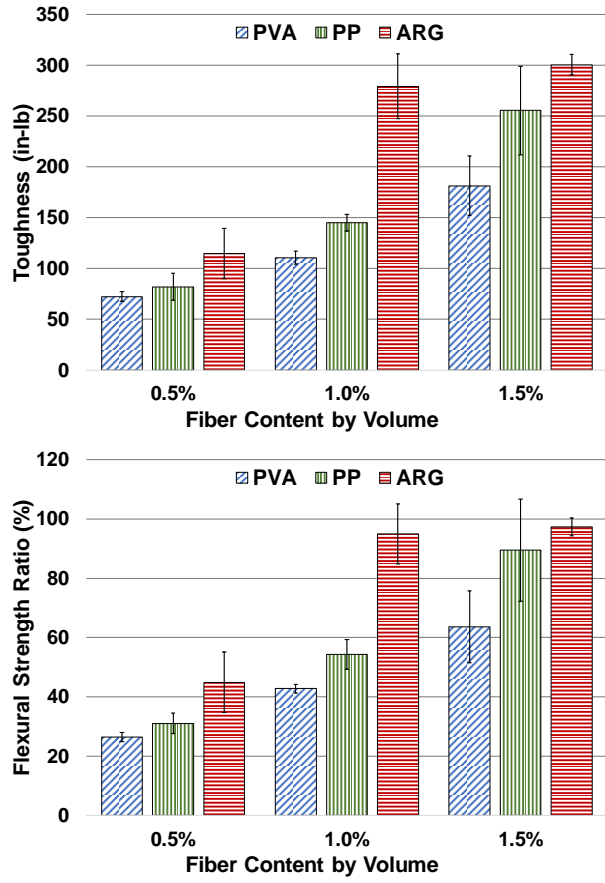


FIGURE 7. Comparisons of (a) toughness and (b) equivalent flexural strength ratio obtained for the three fibers tested in this study (1 in-lb = 0.113 Joules).

CHAPTER 3. DIRECT TENSILE BEHAVIOR OF FIBER REINFORCED CONCRETE MATERIALS FOR DURABLE LINK SLABS

3.1. Direct Tensile Demand

Due to the frequent and costly maintenance requirements associated with bridge expansion joints, the use of link slabs is a promising alternative. Link slabs provide a continuous deck system over simply supported girders, thereby eliminating expansion gaps over intermediate piers that are a major route of ingress for corrosive materials which cause pre-mature degradation of the bridge structure. Link slabs can be subject to a unique combination of structural loads that can cause high tensile stresses in the link slab section (Caner and Zia (1998), Okeil and ElSafty (2005), Ulku et al. (2009)). In order to construct link slabs that can meet the expected serviceability requirements caused by these stresses, materials that can limit crack widths on the slab surface and avoid corrosion are of rising interest.

Traditionally, and in many designs today, conventional concrete with steel rebar is utilized for link slab construction, however this configuration has been shown to develop a single wide crack which although to a lesser extent, would still allow the ingress of corrosive material similar to an expansion joint (Wing et al. (2005)). In order to minimize the crack widths and rebar corrosion in the link slab, design improvements can be achieved by optimizing reinforcement patterns and utilizing recent advancements in cementitious and reinforcement materials.

Engineered Cementitious Composites (ECC) that contain only fine aggregate as well as high volumes of fly ash and polyvinyl alcohol microfiber which causes the material to exhibit high tensile ductility facilitated by the formation of multiple, narrow and tightly spaced cracks have been utilized for link slabs with varying success (Wing et al. (2005), Li et al. (2008)). Major limitations of ECC for link slab applications include difficulties achieving consistent properties in large scale batches, high shrinkage potential, as well as long cast-in-place curing times that are not conducive to accelerated construction schedules.

Due to the limitations of conventional concrete or ECC as link slab materials, previous work related to the current study developed a cast-in-place, high early strength, fiber reinforced concrete (FRC) material consisting of 1.0% volume of ARG macrofibers to accommodate crack control within the link slab (Li et al. (2008)), as well as accelerating and shrinkage reducing admixtures to provide early age strength and shrinkage control in order to accommodate use as a cast in place material for accelerated bridge construction (ABC) link slab projects (Dopko et al. (2018)).

Ultra high performance concrete (UHPC) is a common material for ABC projects as it is typically used for field cast connections between pre-cast elements of the structure. UHPC can be generally characterized as a cementitious material with compressive strength of over 20 ksi. Steel microfiber can be added to UHPC to impart tensile properties that are similar to the previously described tensile properties of ECC, although less ductility can be expected in this type of UHPC compared to ECC. Limited reports describe the use of UHPC for link slabs, however their performance to date is promising (Graybeal (2017)).

Reinforcement materials and placement details are another way to improve the performance of link slabs. Although steel rebar is commonly used for link slab construction, sensitivity to corrosion may inhibit the service life of such structures. Due to this limitation, non-metallic reinforcement that is not sensitive to corrosion could be a sensible substitution for steel rebar in link slabs. One of the most common non-metallic forms of rebar is glass fiber reinforced polymer (GFRP) which has been the subject of recent research efforts (Goldstone et al. (2016), Fava et al. (2016), Yan et al. (2017)). Advantages of GFRP rebar include, decreased self-weight and superior corrosion resistance compared to steel rebar. The tensile stress-strain behavior of GFRP rebar is quite different than that of steel rebar, as GFRP lacks a plastic region. The elastic modulus of GFRP is about 20% of that of steel, however the ultimate tensile strength is well above the typical yield strength of steel rebar.

The relatively low initial stiffness of GFRP rebar may not be conducive to small crack widths when constructed with regular concrete materials (Gu et al. (2016)), however there is evidence showing good composite performance in terms of cracking and flexural load resistance when GFRP rebar is used to reinforce fiber reinforced UHPC materials (Ferrier et al. (2015)). Similarly, Larussen found that the reduced stiffness of GFRP rebar was suited well for use in ECC link slabs due to compatibility with the inherent tensile properties of the ECC (Larussen et al. (2013)).

The limited but significant reported differences in behavior between different combinations of reinforcement and fiber reinforced cementitious materials under tensile stress and the prospective use of such material combinations for link slabs are the inspiration for the current study. Two sizes of epoxy coated steel and GFRP rebar are embedded in concrete, FRC and fiber reinforced UHPC then subject to uniaxial tensile loading, using large dog-bone shaped test specimens. Cracking characteristics, rebar stress, and global displacements will be monitored under displacement controlled loading in order to draw conclusions about how different classes of cementitious materials (i.e. brittle, strain softening, and strain hardening) behave when tested in a composite reinforced with steel or GFRP rebar. The outcomes of this study should provide valuable insights into the fundamental tensile behavior of these composite materials, furthermore evaluating their use as link slab materials in order to provide ABC link slab material design recommendations.

3.2. Experimental Program

3.2.1. Materials

The FRC mixture design used in the current study was developed in related previous work in which optimal macrofiber material and volume dose (Dopko et al. (2018)), as well as high early strength properties for ABC (Dopko et al. (2018)) were determined. In order to assess the effect of fibers in the composite system with rebar, the control concrete mixture used in the current study is of the same matrix as the previously described FRC mixture, only without the 1.0% volume of ARG fibers and an equal volume of fine aggregate added in its place. ARG fiber properties are presented in Table 4. Type I/II Portland cement was used with 20% replacement with Class C fly ash. Accelerating and shrinkage reducing admixtures were included in each mixture in order to maintain consistency with previous related work (Dopko et al. (2018)). A

weight of water equal to the weight of added shrinkage reducing admixture was removed from the mixing water as per manufacturer's recommendation. The shrinkage reducing admixture addition was counted as part of the mixing water weight. The resulting adjusted water to cementitious materials ratio was held constant at 0.38. 3/8 inch crushed limestone was used for coarse aggregate and river sand was used for fine aggregate while the water to cementitious materials ratio was held constant at 0.38. Mixture proportions for the concrete and FRC materials can be found in Table 5.

The UHPC mixture used in the current study is the Iowa DOT UHPC standard joint mixture and includes Ductal JS1000 premix material, water, superplasticizer and 2.0% volume of steel fiber. Properties of steel fibers used in the UHPC mixture can be found in Table 4. Mixture proportions for the UHPC material used in this study can be found in Table 5.

The steel reinforcement used in the current study is standard epoxy coated grade 60 rebar with minimum yield and ultimate strengths of 60 and 90 ksi respectively. Epoxy coated rebar is chosen since it would likely be more representative of in-situ link slab construction due to the corrosion resistance provided by the epoxy. The GFRP reinforcement chosen for the current study has a ribbed surface to increase bond properties similar to steel rebar. Properties of the steel and GFRP rebar are presented in Table 6.

3.2.2. Test Methods

The focus of the current study is on the tensile behavior of different types of cementitious materials when used in a composite system with steel and GFRP rebar. In order to achieve the appropriate loading configuration, large dog-bone shaped specimens are utilized. A single rebar outfitted with a strain gauge at mid-length is embedded in the center of the specimen cross section over the full length of the specimen. Two 5/8 inch diameter threaded steel rods are embedded symmetrically into each end of the specimen to a depth of 10 inches and left to protrude 2 inches from the specimen ends. Details of the dog-bone specimens and the location of the embedded steel are shown in Figure 8. Steel T's with holes cut in their flanges that are symmetric to the spacing of the threaded rods protruding from the dog-bone specimen are clamped into the testing machine by their webs. The specimen is then fastened to the steel T's using the four protruding threaded rods and accompanying steel nuts. Care is taken to ensure the alignment of the specimen is plumb in the vertical axis by adjusting the nuts fastened to the threaded rods which are inserted through the holes in the steel T's. In order to prevent slippage of the rebar in the ends of the specimen, each end of the specimen is clamped together in the horizontal direction, perpendicular to the plane shared by the threaded rod and rebar. Clamps are spaced 15 inches from each other, measured along the active zone (narrow portion) of the specimen. The average displacement in the active zone is measured using two string pot style LVDT sensors fastened to the steel clamps on the specimen using small steel C shaped clamps. Rebar strain is measured using a strain gauge that has been attached to the middle of the rebar length prior to concrete casting. LVDT and rebar strain readings are collected through an external data acquisition system. Surface cracking patterns are monitored by capturing an image every second for the duration of the test using a 22 megapixel camera aligned perpendicular with the face of the specimen active zone. Figure 9 shows the full testing configuration.

Uniaxial tensile tests on dog-bone shaped specimens are performed using a 400k capacity MTS machine and external data acquisition system. Specimens are adjusted using nuts attached to the four protruding threaded rods at specimen ends in order to ensure the specimen is plumb in the vertical direction. Proper specimen alignment and nut adjustment is important to avoid initial bending in the specimen. The specimen is tested under displacement controlled loading at a rate of 0.02 inches/minute until a displacement value of 0.2 inches, after which displacement is increased to 0.1 inches/minute until failure. Tensile tests are performed 7 days after casting. Specimens are de-molded 24 hours after casting and allowed to cure at 73°F and 100% relative humidity.

The standard procedure for concrete compressive strength of 4 inch diameter and 8 inch long cylindrical specimens outlined in ASTM C39 was utilized for all compressive tests. All compression tests were performed on 400k capacity Test Mark hydraulic stroke compression testing machine. Compression tests are performed on the cylinders at 3 and 7 days after casting for all mixtures in order to monitor the strength history of the materials for ABC considerations. The sealed cylinders were cured in 73 °F then de-molded after 24 hours and allowed to cure at 73°F and 100% relative humidity.

3.3. Findings

The plots of the results include a naming convention for each rebar and concrete material combination and can be understood as follows; concrete material – rebar size – rebar material. For example, the data series labeled FRC3S would correspond to fiber reinforced concrete with a number 3 steel rebar and C3G would correspond to concrete with a number 3 GFRP rebar. The plot of load vs. average displacement measured by the two LVDT sensors is presented in Figure 10. Figure 10a shows the plot for LVDT displacements below 0.2 inches, while Figure 10b shows the plot for the entire range of collected data. From the limited data in the figures we can see that the addition of fibers increases the load bearing capacity of the composite section through the range of displacements tested. Another interesting feature from Figure 10 is that the drop in load at the formation of a crack is significantly reduced when fibers are present compared to the control mixture.

The plot of rebar strain vs. LVDT displacement is shown in Figure 11. The plots are nearly linear for specimens including fiber up to near the yield strain of the rebar, which is expected, however the C3S specimen did not follow the same trend. The plot of load vs. rebar strain is shown in Figure 12. The plot only includes data up to the yield stress of the rebar because in service link slabs are to be designed within the elastic region of the reinforcement and seismic designs are outside the scope of this work. The plots in Figure 12 further show how the presence of fibers significantly decreases the strain in the rebar when a crack forms. It can also be seen that fiber mixtures increase the post crack load bearing capacity of the section for a given rebar strain. Photos of the specimens have been collected every second through the duration of the tests in order to monitor cracking behaviors.

More data is needed in order to draw firm conclusions about the data collected, however there is evidence within the current data that the presence of fiber plays a significant role in the reinforcing behavior of steel rebars.

TABLE 4. Fiber properties.

Fiber Type	ARG (FRC)	Steel (UHPC)
Diameter (in)	0.026	0.008
Length (in)	1.7	0.5
Tensile Strength (ksi)	157	300
E. Modulus (ksi)	6382	29000
Specific Gravity	2.1	7.85

TABLE 5. Mixture proportions.

Mixture	Cementitious (lb/cy)			Aggregate (lb/cy)		Admixtures (lb/cy)		
	Type I/II Cement	Class C Fly Ash	Water	Coarse	Fresh	HRWR	Accelerator	Shrinkage Reducer
Concrete	680	170	315	1545	1266	2.4	4.0	8.1
FRC	680	170	315	1545	1218	4.3	4.0	8.1
	Ductal JS 1000 Premix (lb/cy)			Water (lb/cy)		HRWR	Steel Fiber (%)	
UHPC	3700			219		51	2.0	

TABLE 6. Properties of reinforcing bars.

	Steel	GFRP
Ultimate Tensile Strength (ksi)	90	120
Yield Strength (ksi)	60	-
Allowable Tensile Strength (ksi)	-	28
Elastic Modulus (ksi)	29000	6000

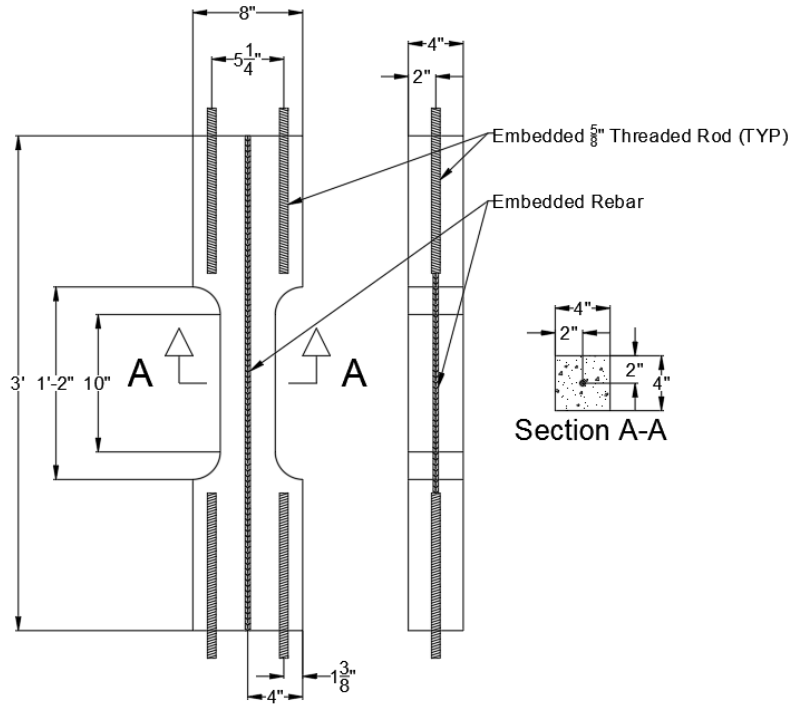


FIGURE 8. Dog-bone test specimen dimensions.

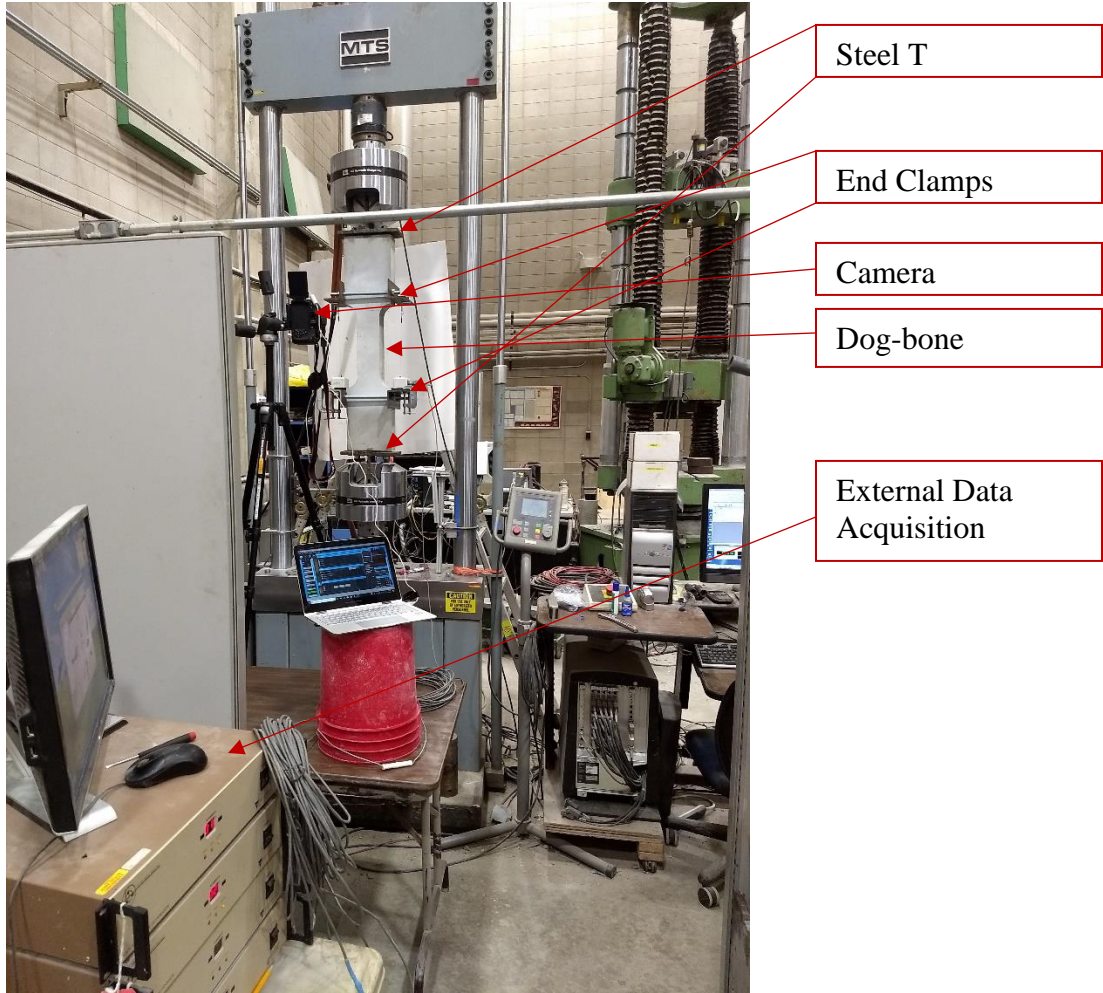


FIGURE 9. Direct tensile test set-up.

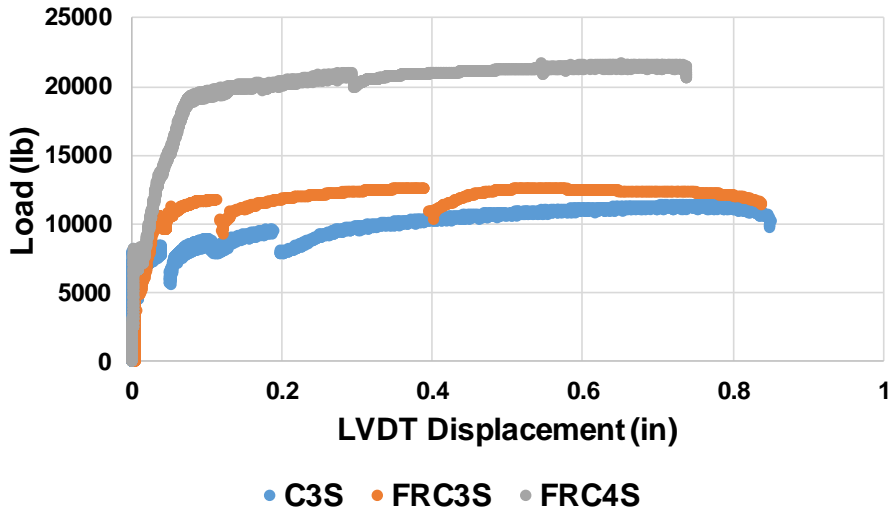
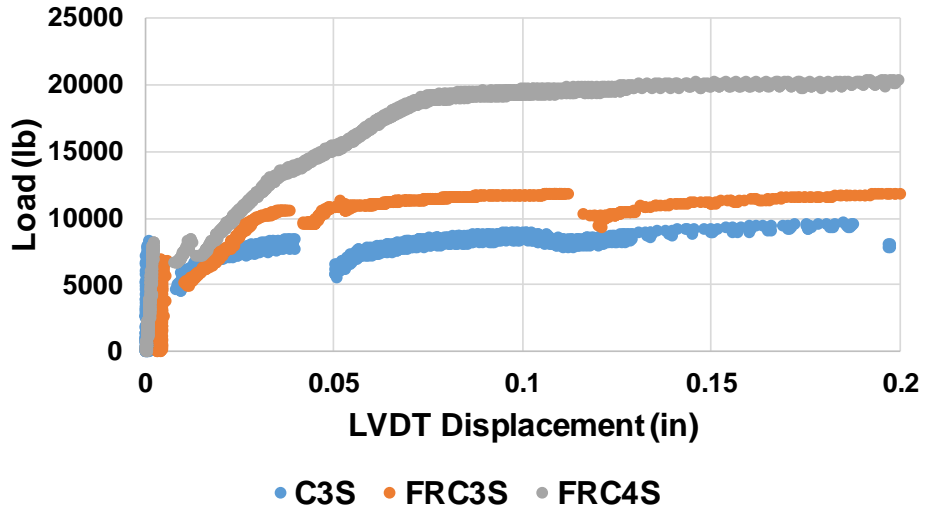


FIGURE 10. Load vs. average LVDT displacement a) up to 0.2 in displacement b) full displacement range.

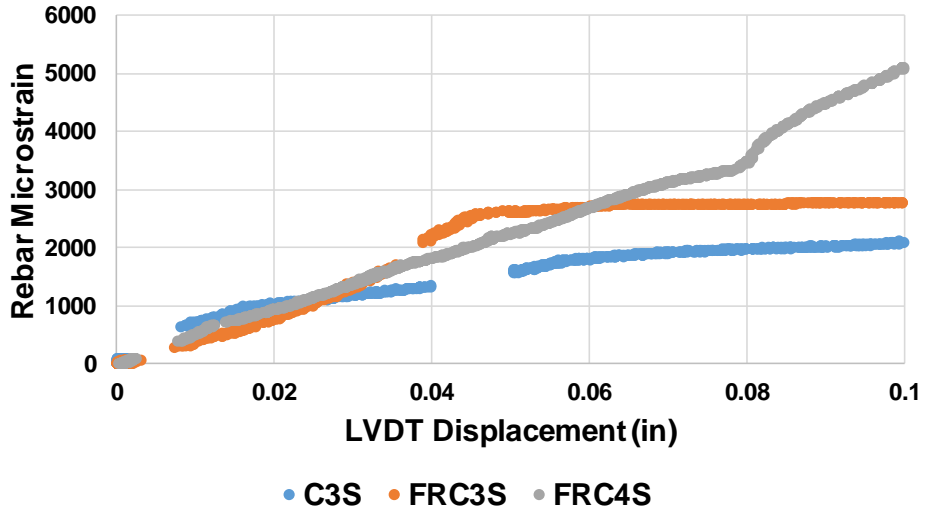


FIGURE 11. Rebar microstrain vs. average LVDT displacement.

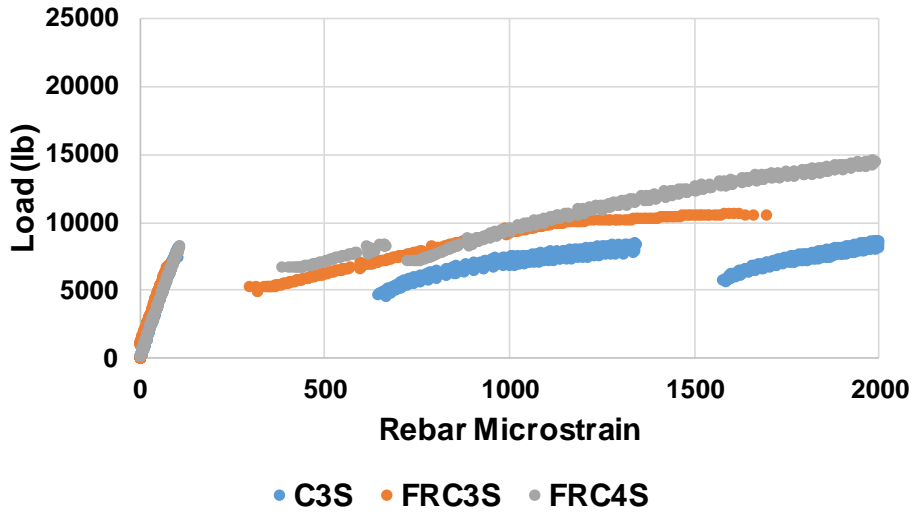


FIGURE 12. Load vs rebar microstrain up to rebar yield strain.

CHAPTER 4. FULL-SCALE STRUCTURAL TEST ON LINK SLAB

4.1. Experimental Setup

A full-scale test was conducted on a link slab in the ISU's Structures Laboratory. The specimen consist of two 21 ft., W21×55 A36 steel girders. The steel girders support a concrete deck with a thickness of 8 inches. The concrete had a strength of 6 ksi on the day of testing. A two-inch gap is provided between the steel girders that represents the expansion joint. A half depth link slab is constructed using fiber reinforced concrete (FRC). The half depth link slab is easy to implement in the field, especially for ABC rehabilitation projects. The FRC is chosen because of high ductility and tension stiffening in tension member and the fact that the FRC minimizes the crack width and often no or very low splitting crack. The FRC had a strength of 8 ksi on the day of testing. The depth of link slab is 4 in, width 63 in and a total length of 67 in. The reinforcement ratio in link slab is 0.011 (Tables 7 and 8). The entire test setup includes strain gages, embedded concrete strain gauges, surface strain gauges, DCDTs and LVDTs. A schematic view of the entire test setup is provided in Figure 13. Figures 14-16 show the reinforcement mat and bridge specimen constructed in the laboratory.

The bridge superstructure is instrumented with strain gauges mounted on rebars in different locations to monitor the evolution of strains induced in the reinforcement during the loading. The strain gauges were installed on the top layer of reinforcement over the support in the deck approaching link slab, on the rebars inside the bonded zone, and on the reinforcements in the debonded zone. This is to monitor the strain variation along the depth of the link slab in both the bonded and debonded regions. Moreover, two surface strain gauges are placed at the top of the debonded surface spaced at 12 in from the centerline of the link slab under the plastic sheeting. Additionally, surface strain gauges are also installed on the surface of the link slab and that of the finished deck. Six linear differential variable transformers (LVDTs) are installed on the steel girder, three on each girder to monitor the curvature of the girder under different support conditions. The instrumentation and debonding of link slab are illustrated in Figure 17. Three direct current displacement transducer are installed one to measure crack width across the centerline of link slab, and at the line where bonded and debonded regions meet. The LVDT's and surface strain gauges can be seen in Figure 17.

4.2. Testing Procedure

The testing procedure involves two types of testing. The first set of testing is conducted to determine the effect of support conditions on the structural behavior of link slab. This set of testing involves loading the entire structure within the elastic limit and recording strains at interface of concrete deck and FRC link slab, at the level of reinforcement in link slab, and on the surface of the link slab for each support configuration.

A load of 20 kips was applied at midspan of each individual span using two actuators. The load of 20 kips was selected based on the load vs deflection curve obtained from the finite element analysis. Once the most critical case was confirmed, the second test was conducted. In this test, the entire structure is loaded to failure. The laboratory test setup and arrangement can be seen in Figure 18.

4.3. Results and Findings

The test result for elastic and ultimate loadings are presented below.

4.3.1. Support conditions

The variation in support conditions caused variation in the beam profile, strain on the top surface of the link slab and strain in the rebar in the link slab. Figure 19 shows that the strain in the top surface of the link slab at the center of the debonded region. The strain is lowest for HRRH support condition and highest for the RHHR support condition, where H represents a hinge support and R represents a roller support. The HRRR support condition, which is a rare support condition in the field showed very close values of strain to that of HRRH boundary condition. Figure 20 shows the strain in the rebar in the link slab. The center of the rebar is located at 2 in from the top surface of the link slab. The strain measured is lowest for HRRH support conditions, and highest for the RHHR support condition. The strain is very close for the HRRH and HRRR cases.

4.3.2. Beam Profile

The deflected shape of the beam under different support condition was different. The RHHR support condition showed the minimum deflection and HRHR support condition showed the maximum deflection. The support conditions HRRR, HRRH, and RHHR had very close values of maximum deflection. The maximum deflection values are shown in Figure 21.

The profile of the beam was observed from the deflection values obtained at three points on each span. The values were then graphed to see the profile of the beam. Figure 22 shows the profile of the beam in a graphical form. The beam profile for the HRHR case provided the lower bound and the RHHR support condition provided the upper bound for the deflected shape of the beam.

4.3.3. Crack width and crack propagation

The crack width was monitored by Direct Control Displacement Transducers (DCDT). The crack first crack initiated through the middle of the debonded region and the crack width reached the minimum AASHTO limit of 0.0118 in, when the loading reached 136 kips (68 kips in the middle of both spans). The crack patterns at the ultimate stage are shown in Figure 23.

The first crack was followed by two other cracks across the link slab at the spot where bonded region ends and debonded region starts. The cracks can be seen in Figure 24. These cracks also extended down to the surface of the concrete deck when the load reached 86 kips. The cracks were all consolidated in the debonded region. At ultimate there were a few cracks in the bonded region.

4.3.4. Strain in Bonded and Debonded Region

Table 9 details the strain values at the ultimate stage in bonded and debonded regions along the height of the link slab. The strain in bonded and debonded regions increase towards the top of the link slab both in bonded and debonded regions. The strain in the debonded region was higher in each level. The strain variation is not linear along the height of the link slab.

4.4. Findings

The following finding can be drawn from this experimental test.

- The support conditions greatly affect the strains and stresses in the link slab. The HRRH case provides the lower bound while the RHHR case provides the upper bound.
- The strains in the bonded region both in the concrete and rebar were significantly less than the strain in the debonded region, which demonstrates the effectiveness of the bonded region in transferring the stresses to the debonded region.
- The strain profile along the height of the link slab shows that the strain distribution in the debonded region varies significantly, while it is almost linear in the bonded region.
- The small width of cracks and the consolidation of small cracks in the debonded region shows the effectiveness of the FRC material of choice in limiting the crack widths and providing additional resistance.

TABLE 7. Reinforcement details for the deck slab.

	Top	bottom
Longitudinal Rebars	#4@ 12 in c/c	#6@ 10 in c/c
Transverse Rebars	#6@ 10 in c/c	#6@ 10 in c/c

TABLE 8. Reinforcement details for the link slab.

	Bonded Region	Debonded Region
Longitudinal Rebars	#6@ 3.5 in c/c	#6@ 7in c/c

TABLE 9. Strains at the ultimate stage.

	Bonded	Debonded	Bonded
Surface strain	2420	12423	2302
In the rebar	1842	4458	1661
Top of debonded surface	753	3875	962

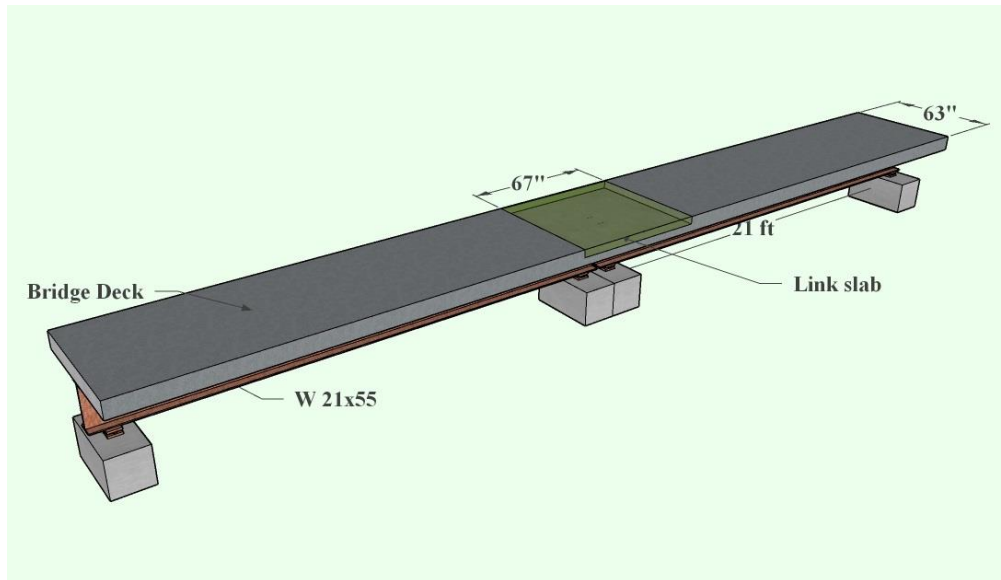


FIGURE 13. A schematic view of the entire test setup.

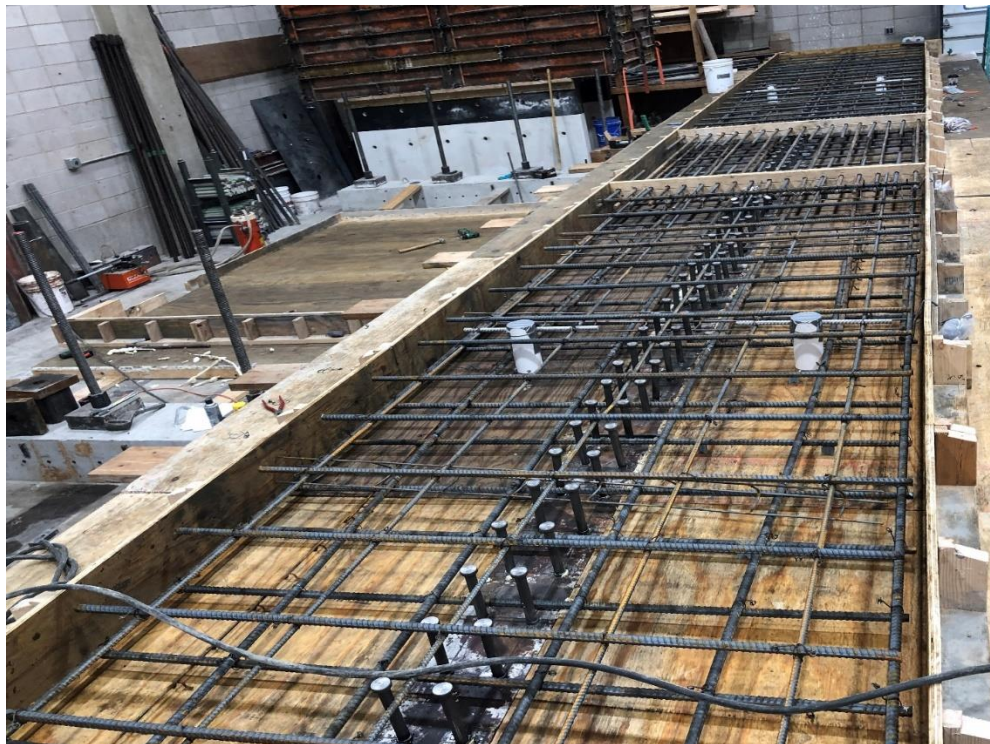


FIGURE 14. Slab reinforcement.



FIGURE 15. Reinforcement in the link slab.



FIGURE 16. Instrumentation and debonding of the link slab portion.



FIGURE 17. DCDT's and surface strain gauges.



FIGURE 18. Laboratory test setup.

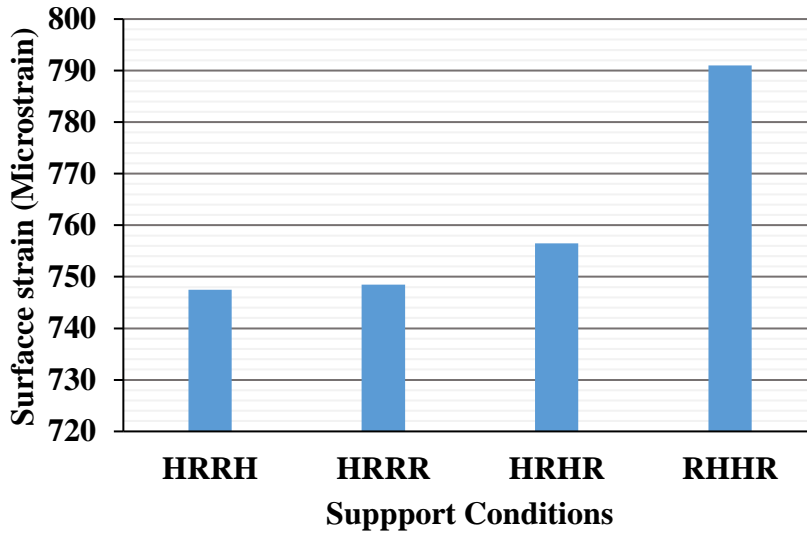


FIGURE 19. Strain in the top surface gauge.

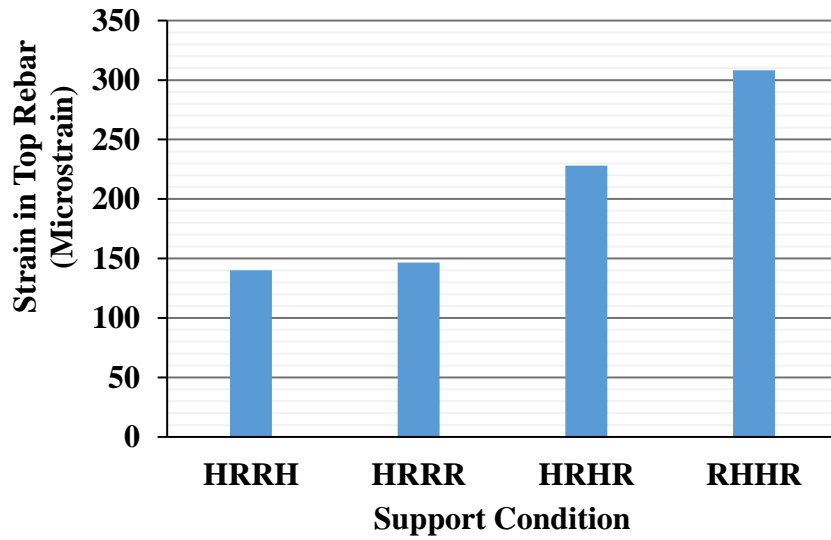


FIGURE 20. Strain in the rebar embedded in the link slab.

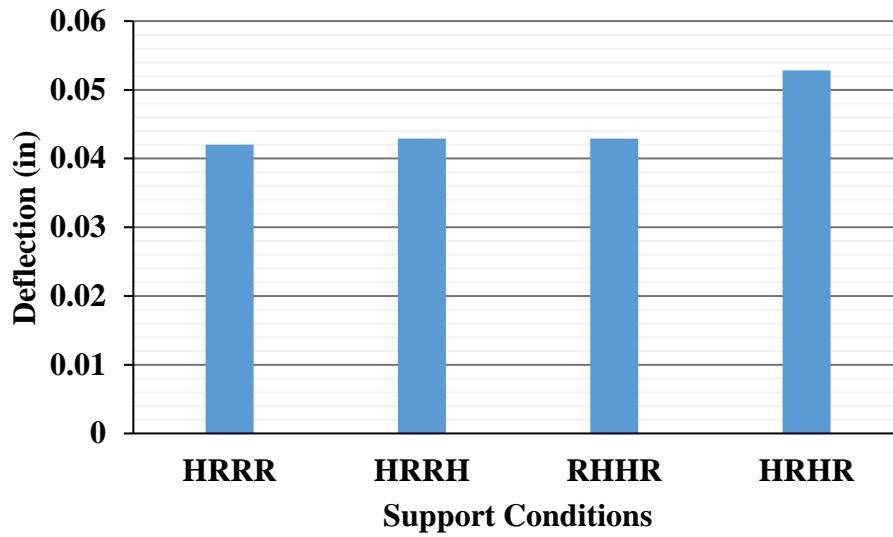


FIGURE 21. Maximum deflection at the center of the left span.

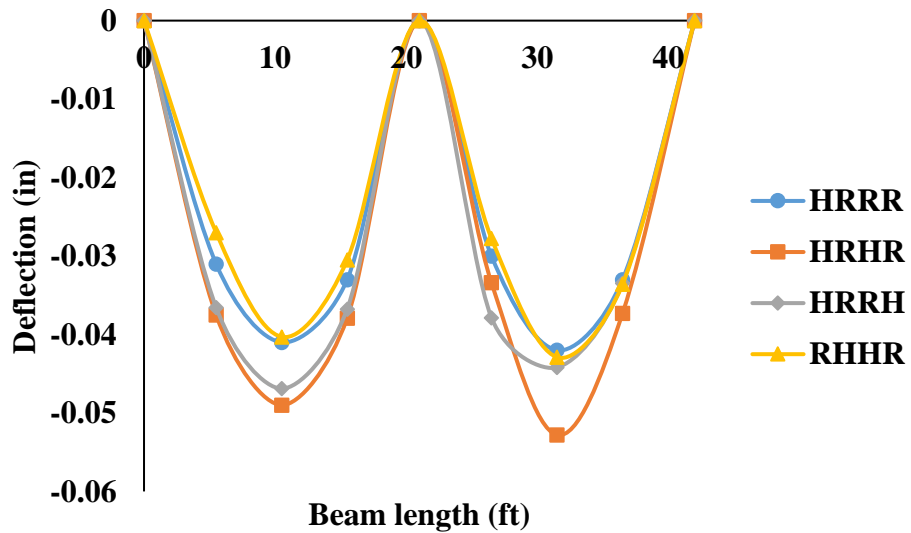


FIGURE 22. Beam profile under different support conditions.



FIGURE 23. Crack pattern in the link slab at the ultimate stage.

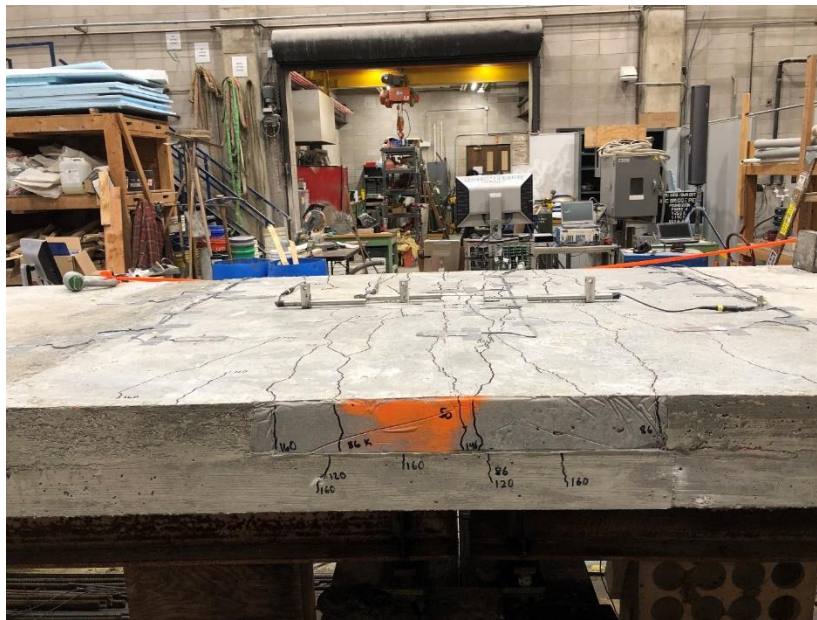


FIGURE 24. Crack patterns in the depth of the link slab at the ultimate stage.

CHAPTER 5. FEASIBILITY ASSESSMENT OF USE OF LINK SLABS IN A CASE STUDY BRIDGE

5.1. Link Slab in Practice

Conventional highway bridges often utilize expansion joints to accommodate movements caused by thermal and service loads. Expansion joints exist over piers between simply supported spans of the bridge and provide a gap for the bridge girder and deck system to rotate, expand and contract. Expansion joints can cause long term durability issues due to the ingress of corrosive materials through the gap they provide which prematurely deteriorates the underlying structure. Debris from the bridge deck can also accumulate in the expansion joint which restricts joint movement and causes damage. Due to these defaults, expensive rehabilitation projects need to be performed on these expansion joints throughout the service life of the bridge. These rehabilitation efforts can be a great burden to State Departments of Transportation due to a lack in funds. For this reason, it is highly desirable to eliminate expansion joints in bridge decks and provide a continuous deck with no gaps in order to avoid these issues. Continuous deck bridges also provide the benefit of a smooth riding surface when compared to steel expansion joint bridges. This is further to the promise of link slabs to expedite the process of bridge construction through Accelerated Bridge Construction (ABC) applications.

Link slabs are a potential solution to the problems associated with expansion joints in bridge decks. Link slabs replace expansion joints over the piers and create a continuous bridge deck system, while maintaining simply supported girder conditions under the deck. Link slabs are typically subjected to high moments and axial forces imposed by thermal and service loading of the supporting girders. Due to this demand, link slabs must be very durable and be able to withstand high tensile loads while being crack resistant to prevent ingress of corrosive materials to the reinforcement and underlying structure. Despite the research efforts that have been made to optimize link slab design and performance, there is a gap in the literature on how to identify candidate bridges, for which the use of link slabs is a reliable solution. This is the motivation of the current study, which explores the feasibility of replacing existing expansion joints of a case-study bridge in Iowa with link slabs. For this purpose, the current study develops a systematic approach to evaluate the structural responses of the case-study bridge with and without link slabs under varying support conditions using the Finite Element (FE) modeling software ABAQUS. The full scale, 3D FE models are utilized to predict the stresses, moments, and forces in each pier of the bridge under positive and negative thermal loading. This information is then analyzed to draw conclusions about how the global bridge structure would react to replacing its two expansion joints with link slabs. The outcome of this study is expected to provide insight into which conditions the installation of a link slab would be advantageous, and which conditions the installation of a link slab would be detrimental to the global bridge structure. The study also expects to provide valuable information on which structural elements of the bridge would be effected most by the presence of a link slab in a multi-span bridge.

5.2. Existing Literature

The concept of using continuous bridge decks over simply supported girders in order to eliminate expansion joints gained attention in the 1980's and 1990's (Zuk (1981), Gastal and Zia (1989),

Richardson (1989), ElSafty (1994)). This research was utilized when the first link slab design methodology and procedure was introduced by Caner and Zia (1998) based on reinforced concrete mechanics and loads induced to the link slab by girder end rotations from maximum mid-span girder deflections (Caner and Zia (1998)). Caner and Zia (1998) performed in-lab point load tests on two two-span, single girder link slab models with varying support conditions. Link slabs were tested with both reinforced concrete and steel girders. Loading was induced in the link slab while reaction forces, deflections and rotations were measured. Two-span, single girder FE models were developed that predicted the responses that were measured in the lab. Once the FE model results were verified with the lab test results, equations were developed for a link slab design procedure. The design methodology and procedure of Caner and Zia (1998) was based on service loading only and the assumption that the flexural stiffness of the link slab was minimal compared to that of the adjacent girders. This led to the idea that the flexural contribution of the link slab to the deck and girder system could be ignored and the link slab could be designed using end rotations conducive to simply supported girder spans. Limit states for this design methodology include crack width criteria and moment demand on the link slab. The design procedure and methodology of Caner and Zia (1998) was put into practice when Wing & Kowalsky (2005) monitored the first bridge to be retrofitted with a link slab in North Carolina in 2005 (Wing & Kowalsky (2005)). This research was the beginning of a number of other full scale field application studies involving link slab retrofits to replace existing expansion joints (Li et al. (2005), Ho et al. (2011), Ozyildirim et al. (2016)).

Due to the unique structural demand on a link slab and the importance of small crack width under service and temperature loads, Kim et al. (2004) investigated using a relatively new type of flexible concrete called Engineered Cementitious Composite (ECC) in link slab applications. ECC utilizes high volumes of fly ash and oiled Polyvinyl Alcohol fiber reinforcement to achieve high tensile strain capacity, tensile strength, post-cracking strain hardening properties, and closely spaced micro-cracking properties. The authors did monotonic and cyclic fatigue testing on ECC link slab specimens in the lab to determine the durability and long term performance of ECC link slabs. It was found that the ECC link slab specimen far out-performed the normal reinforced concrete specimen. Reinforcing bar stresses were smaller in the ECC specimens which could support the idea of lower reinforcing ratios in ECC link slabs. Crack width in the ECC specimens never reached higher than 50 micrometers after 100,000 load cycles while the reinforced concrete specimen showed cracks as high as 640 micrometers. The tight crack width of ECC would be more effective in preventing the ingress of corrosive chemicals, which is the fundamental function of a link slab. The bendable nature of ECC makes it less intrusive on the structure as it should reduce the continuity moment between adjacent girder spans due to lower relative stiffness. The advantages of using flexible ECC materials were well documented and substantial research efforts were deployed to investigate ECC link slabs in greater depth (Li et al. (2005), Li et al. (2008), Li et al. (2009), Ryes and Robertson (2011), Samani (2013), Larruson (2013), Hossain et al. (2014)).

Later work by Okeil & El-Safty (2005) would challenge the assumptions of Caner & Zia (1998) and show that a link slab provides partial continuity between the bridge spans and that the underlying support conditions of the girders have a large effect on the reactions developed in the link slab. Okeil & El-Safty (2005) used FE models to explore the tension force and moment developed in the link slab based on whether the underlying girder supports were roller or hinge

connections. The FE models were of the same dimensions as the models generated by Caner & Zia (1998) in order to provide a fair comparison. Two support conditions were focused on, RHHR and HRRH, where R stands for roller and H stands for hinge. It was found that the RHHR support condition was the upper bound for link slab design due to higher continuity moments and the HRRH support condition was the upper bound for girder design when considering positive moments. These differences were based on the eccentricity of the link slab to the axis of rotation for the RHHR and HRRH conditions. The authors proposed that the inconsistencies in their results compared to Caner & Zia's for support condition effects was due to the fact that Caner & Zia (1998) did not account for inward support movement in the RHHR condition. For each support condition studied, equations for tensile force and continuity moment in the link slab were derived.

Charuchaimontri et al. (2008) used FE modeling to investigate the performance of three common types of link slab reinforcement under increasing loads from expected service loads (AASHTO HS20-44) to ultimate load at failure. The study focused on the relationship between reinforcement and cracking, load/deflection relationship, and ultimate load capacity. In-lab tests were performed to validate the results from the FE models. The authors suggested a revision to the Branson formula (normally used for finding the average effective moment of inertia for simply supported rectangular or T-beams under uniformly distributed load) for calculating the effective moment of inertia for the cracked link slab section based on their results for applied loading. It was found that continuous top and bottom reinforcement showed the best performance results for the link slab.

Ulku et al. (2009) explored the effects of different support conditions, slab debonded length, girder height, and adjacent span ratio using a single girder, two span FE model. Positive and negative temperature gradient loading as well as live load was considered. For support conditions, the HRRR, RHHR and RRHR conditions were investigated. Also, elastomeric bearing pads with different levels of stiffness were modeled using the FE software ABAQUS and investigated for their effect on moment and axial force developed in the link slab. It was found that thermal loading was similar for link slab response when compared to service loading and the authors suggested the use of AASHTO LRFD Service I Limit State design for link slab design. This takes into account live loads and positive or negative thermal gradients. The authors also suggested that an axial force– moment interaction diagram be used for link slab design, similar to that used in reinforced concrete column design.

Further research by Au et al. (2013) used FE modeling, in-lab testing and a full scale live load test on a recently retrofitted link slab bridge to validate the link slab design procedure and investigate the lower limit of debonded length. This research effort focused on service loads only. Live load testing was done to the in-service bridge prior to and after link slab installation for comparison and it was found that the link slab provided partial continuity in the deck superstructure between adjacent girder spans. The presence of the link slab reduced vertical displacements and positive bending moments at girder mid-span and decreased girder end rotations under service loads. These conclusions suggest that a link slab is helpful for the service load capacity of the bridge deck superstructure. When the field measured results were compared to results from the analytical model, it was found that analytically modeled results were always more than field measured results showing that the computational models were conservative. The

analytical model was used to confirm that a 5% debonded length is a practical lower limit. The authors suggested a modification to the link slab design moment equation based on results from their studies by incorporating an adjustment factor to account for the 3D compatibility between the link slab and girder in the debonded region.

There is a current gap in the literature for how the use of link slabs in bridge decks would affect the global structural response, particularly demand on bridge piers. The studies discussed were focused on the behavior and response of the link slab itself, rather than the effects that the use of a link slab may have on the entire bridge. The current study will focus on investigating how the use of link slabs in varying conditions would affect the bridge structure under thermal loads. Positive and negative thermal gradient loading will be the primary focus of the study. Previous studies utilized single girder FE models which could lead to inaccuracies when extrapolating to draw conclusions, especially about reactions in the substructure. This study will utilize full scale 3D bridge models using the FE software ABAQUS. By investigating the structural response of a case-study bridge with and without link slabs, this study will draw conclusions about the feasibility of using link slabs in existing bridge structure.

5.3. Case-Study Bridge

The bridge that was the focus of this research effort has nine spans and eight piers, and is located on Iowa Highway 101 over the Cedar River in Vinton, Iowa (Figure 1a). The net length of the bridge is equal to 811.92 feet. The bridge currently features four expansion joints, two of which are located at the abutments and two of which are located over the third and sixth piers. Continuous supports are located over the remaining six piers, which are assumed to behave closer to an ideal pinned connection than fixed connection. Of the nine spans, the seven interior spans are 96'-6" in length, and the two exterior spans are both 65'-9" in length (Figure 1b). The letting date for the bridge is 1979, making the bridge 37 years of age in 2016. The bridge is constructed from pre-tensioned, pre-stressed concrete beam girders and utilizes deep piling supports at the piers and abutments. The design stresses for the bridge material are in accordance with the AASHTO Standard Specifications for Highway Bridges, Series of 1977: reinforcing steel $f_s = 20,000$ psi (Section 1.5.26B), concrete (girders) $f_c = 5,000$ psi, concrete (other bridge components) $f_c = 3,500$ psi (Section 1.6.6B), and pre-stressing steel $f_s = 270,000$ psi (Section 1.6.6A).

When the bridge was originally designed, the bearing pads that support girders under expansion joints were modeled and expected to behave similar to a roller support. As the bearing pads age, their material properties change. The older the pads get, the more they start to behave like a pinned support rather than a roller support. Taking this and the age of the bridge into consideration when creating the FE model for the case study bridge, it was decided to model the bearing supports as both pinned and roller connections for comparison of responses to a link slab retrofit.

5.4. Finite Element Models

The FE software ABAQUS is used for the FE modeling and simulation in this study. A number of assumptions and idealizations have been made to construct the FE model that can represent

the in-situ bridge as accurately as possible. The most effective 3-D FE model of the superstructure utilizes shell elements for the slab deck with eccentrically stiffened beam elements for the girders (Figure 2). Shell elements are widely used in the FE modeling of slab decks as the behavior of these structural components are governed by flexure. Some studies in the literature have utilized solid elements to model the concrete slab decks. Nonetheless, the most important drawback of the solid elements is the computational time as the analysis time needed for solid elements is several orders of magnitudes longer than that of the shell elements. Since the main focus of this study is to investigate the effects of link slabs on bridge piers, the shell elements are well-suited to model the concrete bridge decks. This minimizes the computational time while maintains the accuracy needed for the modeling of the superstructure. Hence, for the FE models used in this study, the S4R (i.e., a 4-node doubly curved thick shell elements with reduced integration, hourglass control, and finite membrane strains) shell elements are employed to model the concrete deck slabs. The girders are modeled using the so-called B31 beam elements that represent 2-node linear beam in space. To capture the accurate stiffness of girders, the exact cross-sectional geometry of the girders is assigned to them.

The ABAQUS package has the capability to input an offset distance for the shell and beam elements from their node locations. Thus, the shell and beam elements are assigned to the mid-surface and neutral axis of the thickness of slab and cross-sectional area of girders, respectively. This makes it possible to accurately capture the T-beam moment of inertia. The full composite action between the concrete slab decks and prestressed concrete girders is modeled by the node-to-surface links through the tie constraints. Care is taken to tie a portion of deck slab as wide as (at least) the top flange width of each girder. This helps the slab decks and the girders tied to them to act monotonically under external loads as is the case for the in-situ bridge.

For the models with link slabs, the 6 inch expansion gap is filled with concrete materials. The link slabs are modeled using the same materials and elements as the concrete deck slabs in this study. This approach provides the “worst case scenario” in terms of demand under the dead and/or thermal loads. The connectivity between the link slab and slab decks, on both sides, is defined using the surface-to-surface tie constraints. The concrete piers are modeled using the S4R shell elements. Since the concrete piers are the main focus of this study, the mesh size of piers are three times smaller than that of the other structural components included in the model. The connectivity between the piers and the girders are modeled by rigid links through multi-point constraints (MPCs). Such rigid links enforce the kinematic relationships between the degrees of freedom (DOFs) at each node shared with two different types of finite elements, i.e., shell elements of the piers and beam elements of the girders. This will effectively eliminate the perturbation of stresses and strains at the interface boundary of the piers and girders. The boundary conditions (BCs) at the base of the piers are modeled using ideal fixed connections. The effect of BCs on the results are captured by defining roller and pinned BCs at both ends as well as the locations of the expansion joints on the superstructure (Figure 3). Three load cases are defined, including dead load (DL), thermal load (TL) and the combination of the dead and thermal loads ($DL \pm TL$). As for the DL, the self-weight of all structural components modeled in this study are assigned to them. The TL refers to the loads that the bridge components experience when the temperature of the entire bridge structure is increased/decreased by 70 °F. The results of the $DL \pm TL$ are also reported and discussed for comparison purposes.

5.5. Simulation Results

As discussed in the previous section, a full-scale 3D FE model is created using the ABAQUS package to investigate the effects of replacing existing expansion joints over the piers with link slabs. Due to the change in the behavior of bearing pads over time from roller type properties to pin type properties, the girder support conditions under the link slabs are modeled using both pin and roller connections to investigate the upper and lower bounds of the in-situ conditions. Due to symmetry, results from half of the bridge are reported to formulate the following observations.

In the current study, four different FE bridge models are generated and analyzed for three load cases each. The four models have either pinned or roller connections at Pier #3, Pier #6 and the abutments. Also the models either had expansion joints or link slabs at Piers #3 and #6. The following naming convention is given to each model: Roller support without Link Slab (RwoLS), Roller support with Link Slab (RwLS), Pinned support without Link Slab (PwoLS), and Pinned support with Link Slab (PwLS). These abbreviations are used in the following discussions and figures. Positive and negative thermal gradient loading was the focus of this study since expansion joints are principally designed to accommodate thermal loads. The point of interest lies in the situation where a link slab retrofit is used and expansion joints are no longer available to absorb thermal movement. This point was the focus of the results analysis.

Positive and negative thermal loads produced similar results for all support conditions (Figure 4). The stresses, moments, and forces that resulted in each pier under each condition are very similar. As an example, the sum of the vertical stress contribution from bending moment and axial force (total stress) from DL + TL in the RwLS case at Pier #1 is within 7% of the total stress from the DL – TL in the same (RwLS) analysis cases. Since all the results for +TL loading and –TL loading are within 10%, absolute values are used for moments and base shear since thermal movements in opposite directions create moment and shear of opposite sign. Due to the symmetry in the results for positive and negative temperature loads, the rest of this section will focus on the effects of dead load and positive thermal gradient (i.e., DL + TL) on the structural behavior of bridge cases. Figure 5 shows the equal and opposite symmetry in the deformed shapes of the RwLS model under (a) +TL and (b) –TL.

The presence of pinned supports at the abutments and under the link slabs produces relatively minimal stresses, moments and shear forces in the pier bases regardless of the presence of a link slab (Figures 6-8). It can actually be noticed that the presence of a link slab will slightly decrease the total stress, moment and base shear force at the bottom of the piers for the pinned support condition under thermal loads. This could be attributed to the fact that the link slab transfers forces from lateral movement at the top of the deck-girder system between adjacent spans, rather than these lateral reactions being resolved only in the support and consequently the pier. Roller support conditions, however, produce much different results. The roller support condition without the presence of link slabs produces relatively small total stresses, moments and base shear forces in all of the piers. On the other hand, when a link slab is used with roller support conditions, large stresses, moments, and base shear forces are developed in Piers #1 and #2, which are between the link slab and abutment (Figures 6-8). In comparison, under temperature gradient loading, the total stress, moment, and shear force in Pier #1 increases by 90%, 97% and 97%, respectively for roller connections over pinned connections when link slabs are present.

Under temperature gradient loading, the total stress, moment and shear force in Pier #2 increases by 88%, 96% and 97%, respectively. Larger stresses, moments and shear forces are noticed in Piers #3 and #4 for roller connections under temperature loading (TL), but the difference is relatively small and the values are negligible in comparison.

Dead load contributions to moment and shear force in all four piers is approximately one order of magnitude smaller than the contributions of temperature loads. The overall trends that can be captured from the simulation results include: 1) Piers #1 and #2 exhibit high stresses, moments and shear forces from temperature loading when roller support conditions are used, 2) dead load contributions to total stress, moment and shear force are relatively small compared to temperature load contributions, and 3) the change in total stress, moment and shear force with the presence of a link slab when pinned connections are used is very small.

The contributions of temperature load to axial force is found to be small compared to dead load except for the PwoLS case, in which a relatively significant amount of axial force is produced (Figure 9). The PwLS case under temperature loading produces a significant amount of axial force in Pier #1, but none of the other piers. This shows that the presence of a link slab when pinned supports are utilized actually reduces the structural demand in all except the outer-most piers. Dead load was the main contributor to axial force in all piers and in all support and link slab configurations. For the most extreme case, in Pier #3 and the PwoLS case, the ratio of the contribution of temperature loading is still only 36% of the total axial force. This shows that the presence of a link slab does not greatly change the axial forces in bridge piers (Figure 9).

Figure 10 highlights that the deformed shape of the bridge under DL+TL is much different for roller and pinned connections. Although the piers deform substantially with roller connections and consequently experience large bending stresses, moments and base shear forces, the deck-girder system experiences a relatively small deformation. For the pinned connection condition, however, the same loading case would result in potentially excessive stresses in the deck and girders. On the other hand, the presence of a link slab does not cause any substantial effect on the bridge pier in the pinned connection condition. The identification of link slab materials that can manage the loading demand on both superstructure and substructure of bridges is the subject of the next stage of this ongoing research.

5.6. Findings

A full scale FE model of an existing bridge in Iowa was created to investigate the effect of using link slabs to replace expansion joints on the bridge substructure. The obtained results showed that when the bearing pads that support the girders at the abutments and over the piers that are under the link slab are modeled as roller connections, there is a relatively large build-up of stresses, moments and shear forces in the piers between the link slab and abutment (e.g., Piers #1 and #2). When these bearing pads are modeled as pinned connections, it can be seen from the results that the presence of a link slab in place of an expansion joint will have a negligible effect on the stresses, moments and shear forces in all of the piers. A small decrease in the pier stresses, moments and shear forces can even be noticed for this support condition if a link slab is used in place of an expansion joint.

The presented study was primarily focused on the reactions in the piers. Based on the boundary conditions and deformed shape of the bridge when pinned connections are used with a link slab, it can be seen that there would be a stress build-up in the girder and deck system, rather than the piers. Keeping this in mind, the pinned support condition would be the upper limit for girder and deck stress, while the pinned support condition would be the upper limit for pier stresses. Given that in-situ bearing pads act somewhere in between ideal roller or ideal pinned connections, depending on the age of the bearing pads, the actual stress distribution would be shared between the girder-deck system and piers.

As in-situ bearing pads like the pads used on the case study bridge in this study age, they behave less like a roller connection and more like a pinned connection. The presence of a link slab when pinned connections are used would have a small effect on the stresses in the girder-deck system since lateral movement is already restrained by the fundamental definition of a pinned connection, causing a stress build up. Although other solutions may be needed to remediate this stress build up in the girder-deck system, the presence of a link slab would be minimally invasive based on the findings of this study. Given the findings of this study, it may be beneficial to utilize link slabs on older bridges in retrofit situations from a structural and serviceability standpoint.

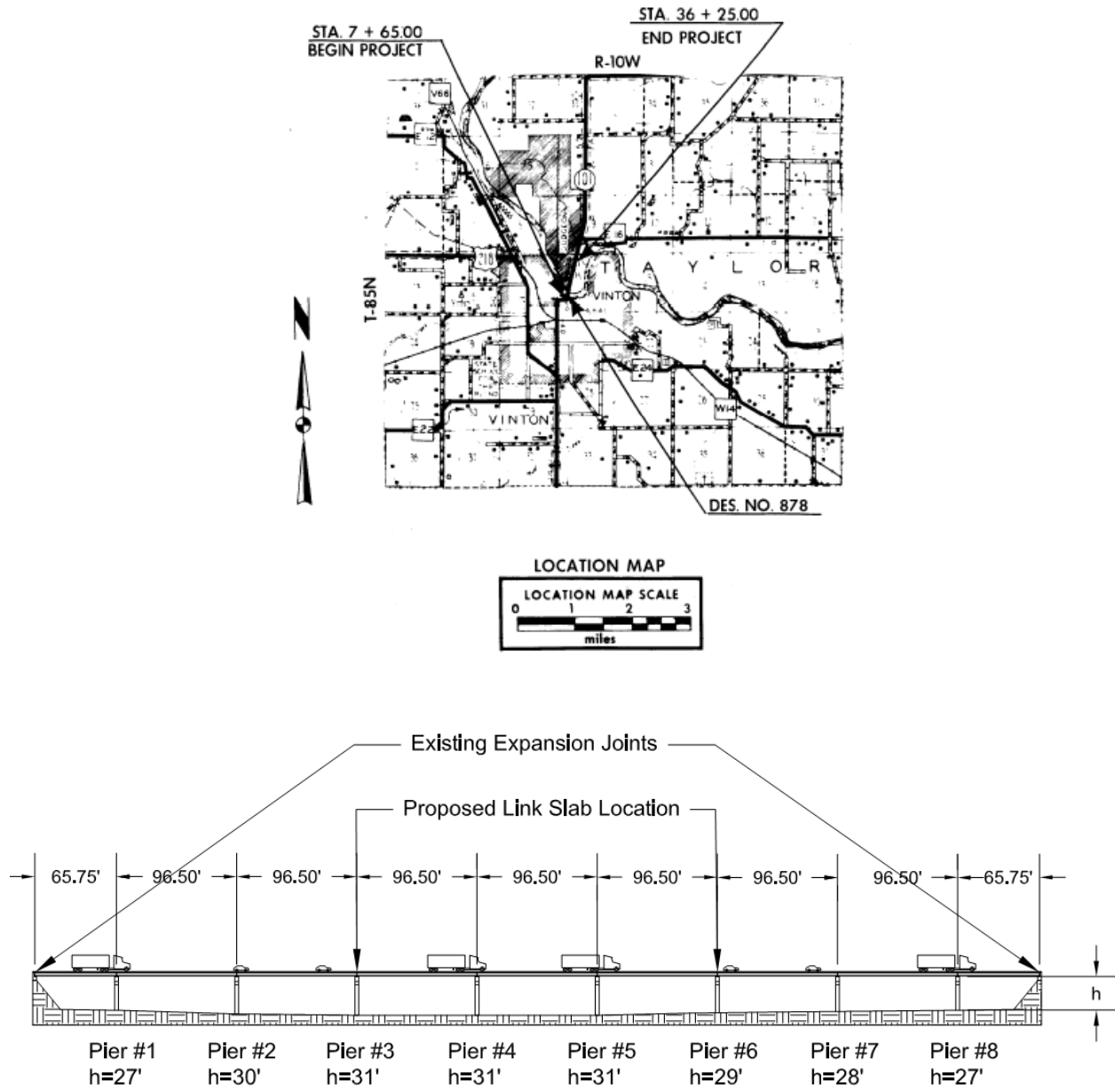


FIGURE 25. Location (top) and schematic layout (bottom) of the case study bridge.

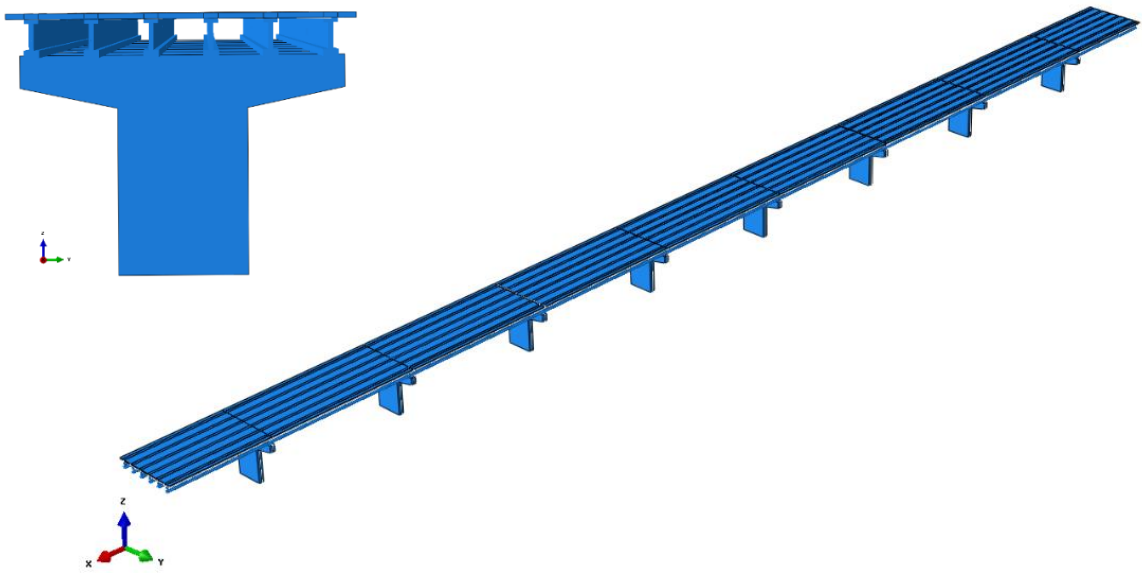


FIGURE 26. Full-scale 3D FE model of the case study bridge.

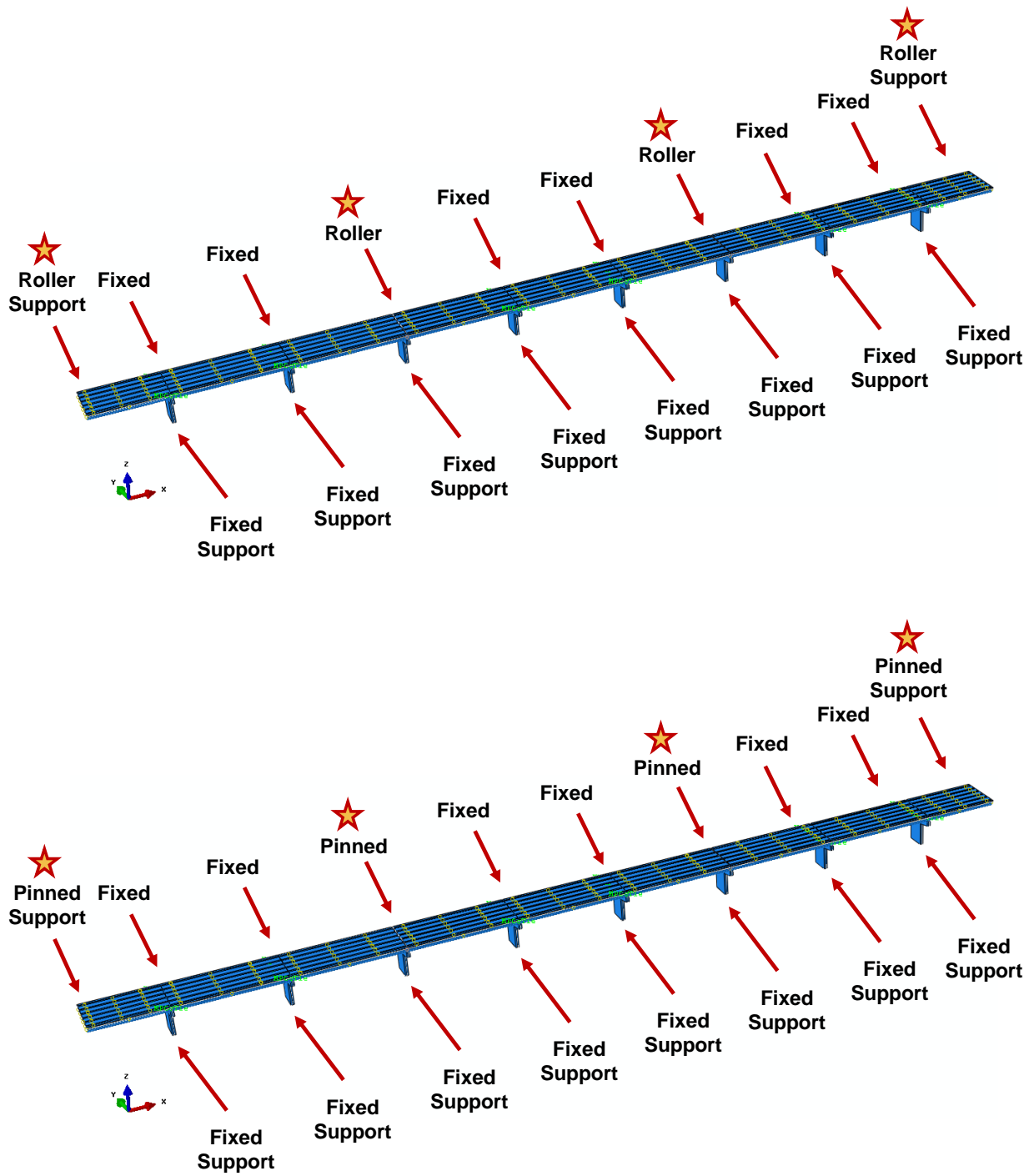


FIGURE 27. An overview of the two sets of BSc used for the case study bridge.

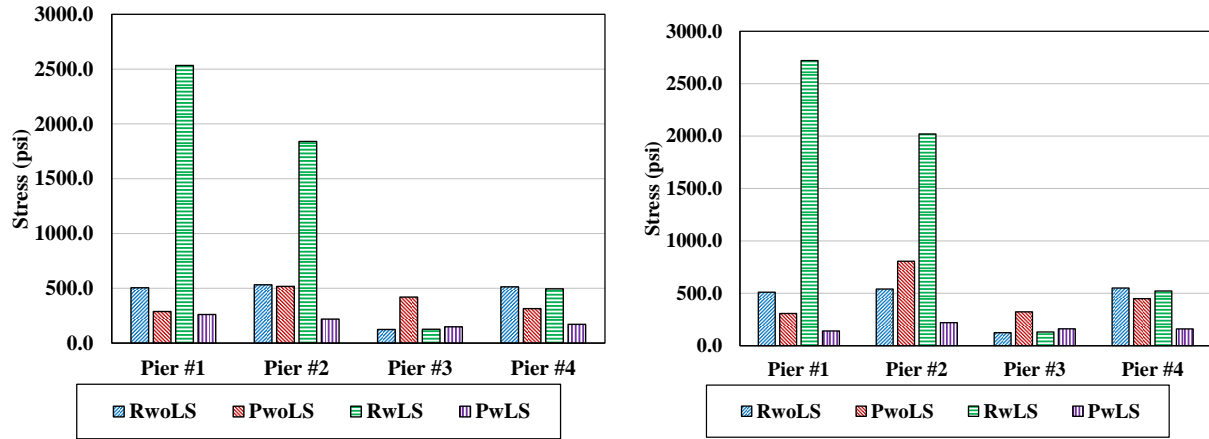


FIGURE 28. Total stress at the pier base: DL + TL (left) and DL - TL (right).

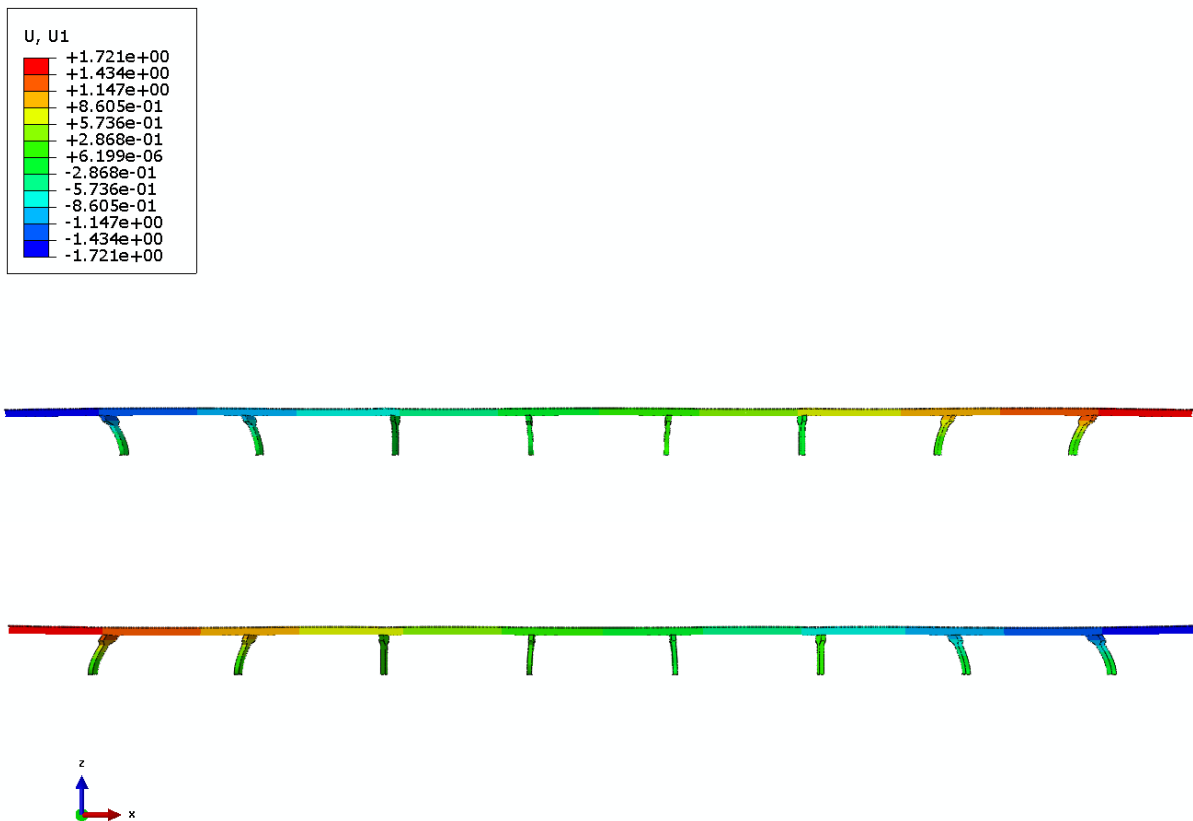


FIGURE 29. Exaggerated deformed shape of the bridge under +TL (top) and -TL (bottom). The deformation unit is inch.

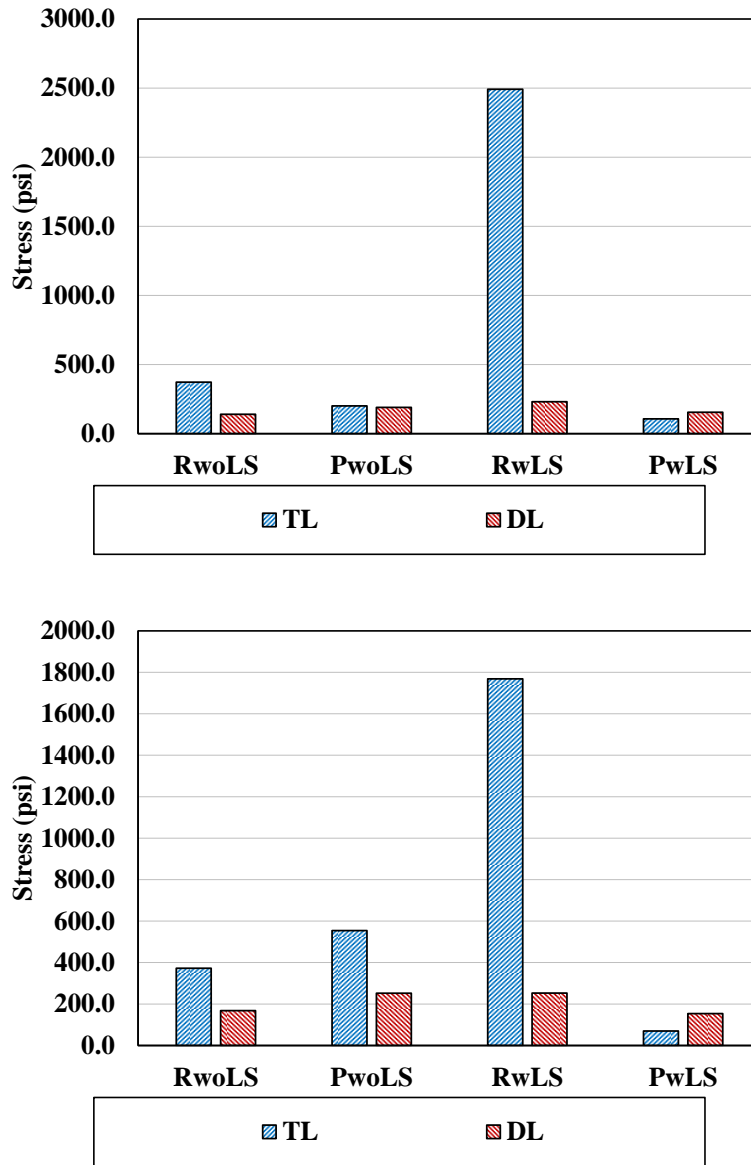


FIGURE 30. Total stress under DL + TL at the pier base: Pier #1 (top) and Pier #2 (bottom).

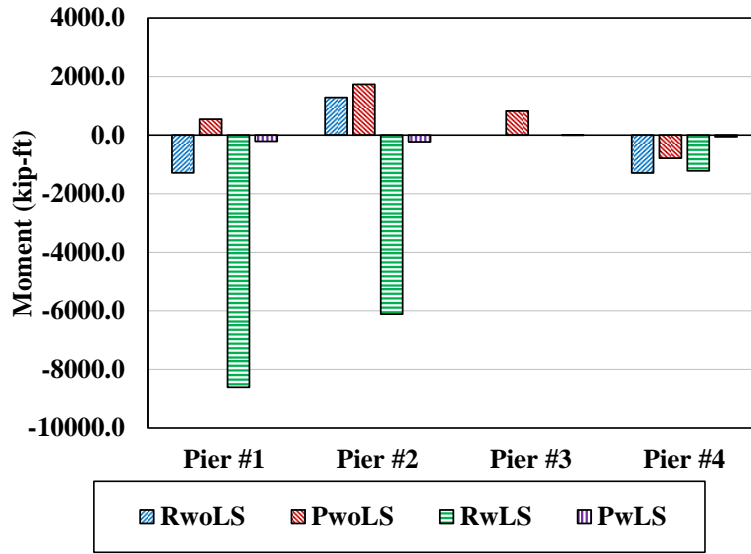


FIGURE 31. Bending moment in the piers for the four cases under +TL.

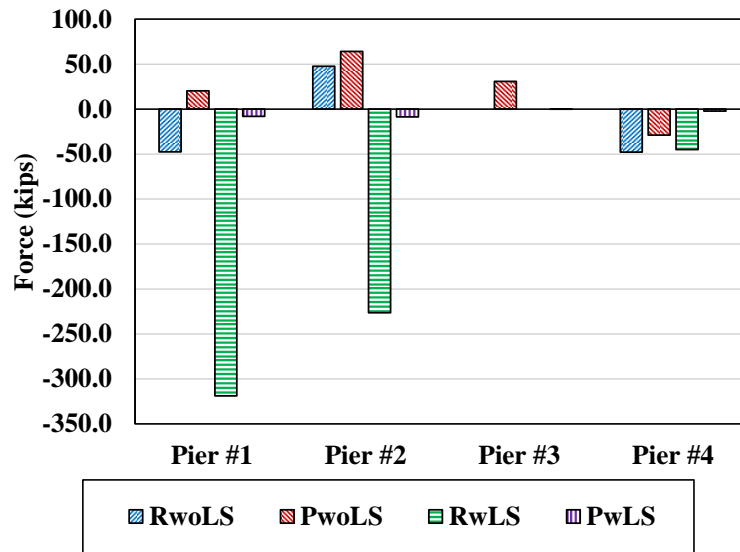


FIGURE 32. Shear force in four piers for the four cases under +TL.

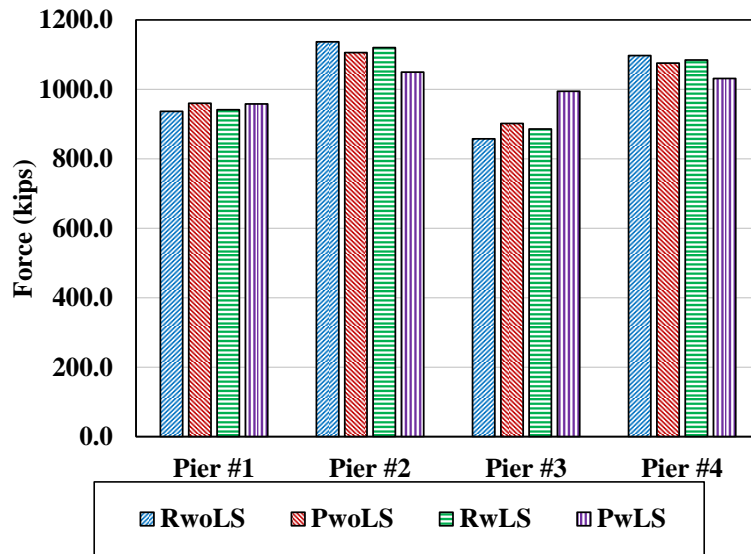
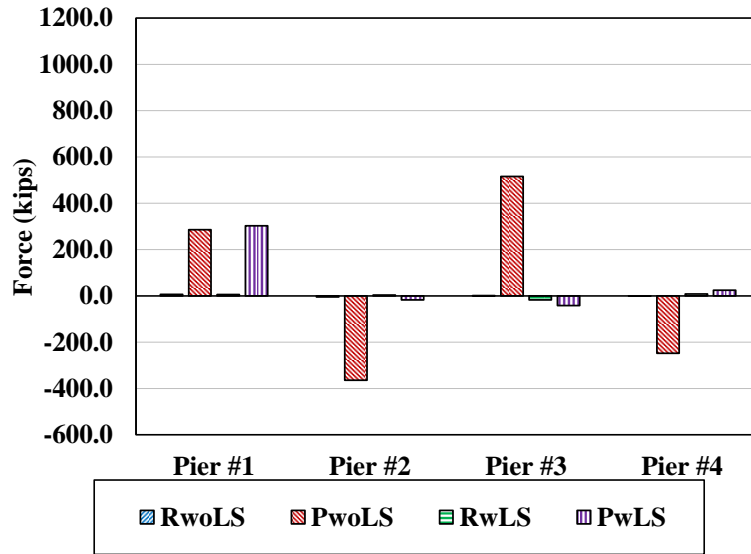


FIGURE 33. Axial force generated at the pier base for the four cases under +TL (top) and DL (bottom)

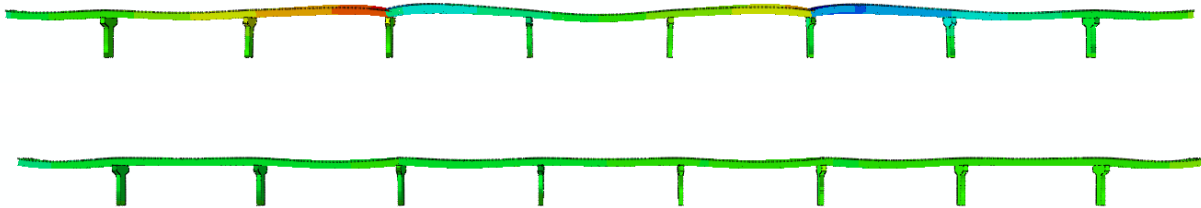
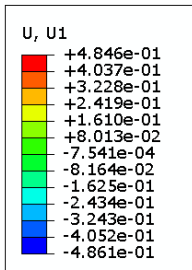
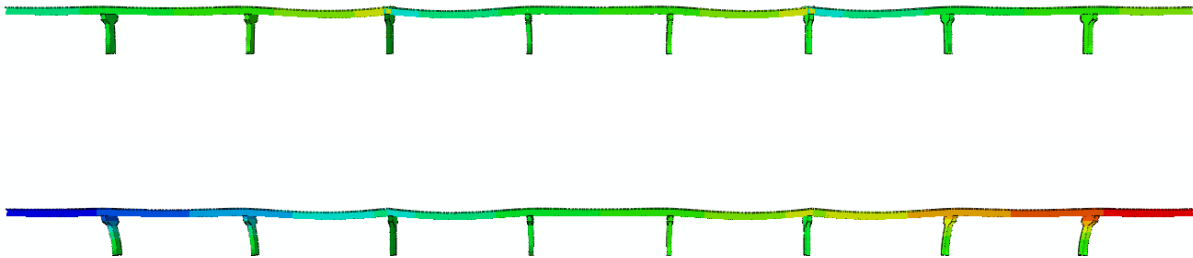
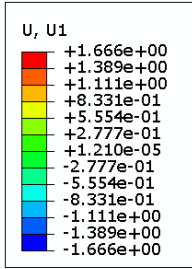


FIGURE 34. Exaggerated deformed shape of the bridge under DL + TL for four analysis cases: RwoLS and RwLS (top two), PwoLS and PwLS (bottom two).

CHAPTER 6. CONCLUSIONS AND RECOMMENDATIONS

6.1. Summary

The use of link slabs in place of bridge expansion joints is a promising solution in terms of performance, economy, and durability. The current report has described an in depth investigation into the use of link slabs with ABC. Link slab material design considerations have been addressed through a comprehensive set of tests on FRC, the outcomes of which provides insight into which FRC mixtures are best suited for ABC link slabs. The developed FRC ABC link slab mixture is further investigated for its tensile behavior and performance compatibility with steel and GFRP reinforcement. A control mixture with no fiber as well as UHPC including steel fiber is also tested under the same configurations and conclusions are drawn as to the best cementitious and reinforcing material combinations for the desired serviceability requirements of ABC link slabs. The study was then extended to a full-scale structural test, which demonstrated the capability of the proposed mix design and structural configuration in minimizing the extent of damage even under an ultimate stage of loading.

6.2. Significant Results and Findings

Through the completion of two experimental studies regarding FRC mixtures for ABC link slab applications and the partial completion of an experimental study regarding the performance of FRC and UHPC in conjunction with steel and GFRP rebar under uniaxial tension, and a case study on use of link slab using finite element complemented by an experimental test in the laboratory these conclusions can be made.

- ARG macro fibers were more effective at increasing flexural toughness and residual strengths than the polypropylene or polyvinyl alcohol fibers tested even though the ARG fibers had a lower aspect ratio, likely due to strong fiber-matrix bond properties provided by the resin coating.
- ARG macro fibers showed much less of an effect on concrete fresh properties compared to polypropylene or polyvinyl alcohol fibers tested at the same volumetric dose, likely due to their slightly smaller aspect ratio and similar density to the concrete matrix. The increased workability of ARG fiber mixtures compared to other tested fibers makes them more conducive to ease of construction and therefore ABC practice.
- FRC with 1.0% ARG macrofiber may effectively increase the load carrying capacity and alleviate strain in the rebar of reinforced concrete after cracking has occurred.
- The pinned support condition will be upper limit for stresses in the girder and deck system while roller support will be upper limit for the pinned support.
- Finite element analysis shows link slabs can be beneficial to be used in retrofit situations.
- The support conditions will affect the strains and stresses in the link slab. The HRRH case provides the lower bound while the RHHR case provides the upper bound.
- The strains in the bonded region both in the concrete and rebar were significantly less than the strain in debonded region, which shows the effectiveness of bonded region in transferring the stresses to the debonded region.

- The strain profile along the height of the link slab shows that the strain distribution in the debonded region varies significantly, while it is almost linear in the bonded region
- The small width of cracks and the consolidation of small cracks in the debonded region shows the effectiveness of the FRC material of choice in limiting the crack widths and providing additional resistance.
- In the case-study bridge, when the piers under the link slabs are modeled as a roller connection, there is relatively large stresses on the piers between the abutment and link slab. When these bearings are modeled as a pin connection, stresses in the pier are reduced to a negligible range. This highlights the importance of boundary conditions assumed for the design and configuration of link slabs.

6.3. Future Work

Future work can include an investigation into the behavior of link slabs made with other materials, such as ultra-high performance concrete and glass fiber reinforced bars designed utilizing the findings from this work. Future work can also involve the implementation of the findings of this project into real bridges and monitor their short and long-term performance.

REFERENCES

- ACI Committee 544. 2009. *Report on Fiber Reinforced Concrete*, ACI 544.1R-96 (Reapproved 2009). American Concrete Institute.
- Alani, A. M., & D. Beckett. 2013. *Mechanical properties of a large scale synthetic fibre reinforced concrete ground slab*. *Construction and Building Materials*, Vol. 41, , pp. 335-344.
- ASTM, C 1609/C 1609M-05. 2005. *Standard Test Method for Flexural Performance of Fiber-Reinforced Concrete (Using Beam with Third-Point Loading)*, ASTM International.
- ASTM Standard C39, 2005. *Standard Test Method for Compressive Strength of Cylindrical Concrete Specimens*. ASTM International.
- Au, A., C. Lam, J. Au, and B. Tharmabala. 2013. *Eliminating Deck Joints Using Debonded Link Slabs: Research and Field Tests in Ontario*. *Journal of Bridge Engineering*, Vol. 18, No. 8, , pp. 768-778.
- Banthia, N., & S. M. Soleimani. 2005. *Flexural response of hybrid fiber-reinforced cementitious composites*. *Materials Journal*, Vol. 102, No. 6, pp. 382-389.
- Bentur, A., & S. Mindess. 2006. *Fibre Reinforced Cementitious Composites*. CRC Press.
- Buratti, N., C. Mazzotti, & M. Savoia. 2011. *Post-cracking behavior of steel and macro-synthetic fibre-reinforced concretes*. *Construction and Building Materials*, Vol. 25, No. 5, pp. 2713-2722.
- Banthia, N., & R. Gupta. 2006. *Influence of polypropylene fiber geometry on plastic shrinkage cracking in concrete*. *Cement and Concrete Research*, Vol. 36, No. 7, pp. 1263-1267.
- Betterman, L. R., C. Ouyang, & S. P. Shah. 1995. *Fiber-matrix interaction in microfiber-reinforced mortar*. *Advanced Cement Based Materials*, Vol. 2, No. 2, pp. 53-61.
- Cao, J., & D. D. L. Chung. 2001. *Carbon fiber reinforced cement mortar improved by using acrylic dispersion as an admixture*. *Cement and Concrete Research*, Vol. 31, No. 11, pp. 1633-1637.
- Caner, A., and P. Zia. 1998. *Behavior and Design of Link Slabs for Jointless Bridge Decks*. *PCI Journal*, Vol. 43, pp. 68-81.
- Charuchaimontri, T., T. Senjuntichai, J. Ozbolt, and E. Limsuwan. 2008. *Effect of lap reinforcement in link slabs of highway bridges*. *Engineering Structures*, Vol. 30, No. 2, pp. 546-560.
- Dopko, M., Najimi, M., Shafei, B., Wang, X., Taylor, P., and Phares, B. 2018. *Flexural performance evaluation of fiber reinforced concrete incorporating multiple macro-synthetic fibers*, Transportation Research Board Annual Meeting, January 7-11, Washington, DC.
- Dopko, M., Najimi, M., Shafei, B., Wang, X., Taylor, P., and Phares, B. 2018. *Assessment of strength and restrained shrinkage behaviors on micro-carbon fiber reinforced concrete with binary chemical admixtures*, Transportation Research Board Annual Meeting, January 7-11, Washington, DC.

- El-Safty, A.K. 1994. *Analysis of Jointless Bridge Decks with Partially Debonded Simple Span Beams*. PhD. Dissertation, North Carolina State University Raleigh, NC.
- Fraternali, F., V. Ciancia, R. Chechile, G. Rizzano, L. Feo, & L. Incarnato. 2011. *Experimental study of the thermo-mechanical properties of recycled PET fiber-reinforced concrete*. *Composite Structures*, Vol. 93, No. 9, pp. 2368-2374.
- Fava, G., Carvelli, V., & Pisani, M. A. 2016. *Remarks on bond of GFRP rebars and concrete*. *Composites Part B: Engineering*, 93, 210-220.
- Ferrier, E., Michel, L., Zuber, B., & Chanvillard, G. 2015. *Mechanical behaviour of ultra-high-performance short-fibre-reinforced concrete beams with internal fibre reinforced polymer bars*. *Composites Part B: Engineering*, 68, 246-258.
- Graybeal, B. A. 2017. *Emerging UHPC-based bridge construction and preservation solutions*.
- Goldston, M., Remennikov, A., & Sheikh, M. N. 2016. *Experimental investigation of the behaviour of concrete beams reinforced with GFRP bars under static and impact loading*. *Engineering Structures*, 113, 220-232.
- Gu, X., Yu, B., & Wu, M. 2016. *Experimental study of the bond performance and mechanical response of GFRP reinforced concrete*. *Construction and Building Materials*, 114, 407-415.
- Gastal, F., and P. Zia. 1989. *Analysis of Bridge Beams with Jointless Decks*. Proceedings of IASBE Symposium, pp. 555-560.
- Hamoush, S., T. Abu-Lebdeh, & T. Cummins. 2010. *Deflection behavior of concrete beams reinforced with PVA micro-fibers*. *Construction and Building Materials*, Vol. 24, No. 11, pp. 2285-2293.
- Hossain, K. M. A., and M. S. Anwar. 2014. *Strength and Deformation Characteristics of ECC Link Slab in Joint-Free Bridge Decks*. Istanbul Bridge Conference.
- Ho, E., and J. Lukashenko. 2011. *Link Slab Deck Joints*. Annual Conference of the Transportation Association of Canada.
- Hulsey JL. 1992. Final report bridge lengths : *jointless prestressed girder BRIDGES* by School of Engineering University of Alaska Fairbanks 263 Duckering Building Fairbanks , AK 99775, Prepared for Alaska Cooperative Transportation And Public Facilities Quic.
- Johnston, C. D. 2001. *Fiber-Reinforced Cements and Concretes*, CRC Press, Vol. 3.
- Kim, Y. Y., G. Fischer, and V.C. Li. 2004. *Performance of Bridge Deck Link Slabs Designed with Ductile Engineered Cementitious Composite*. *ACI Structural Journal*, Vol. 101 No. 6, pp. 792-801.
- Lárusson, L.H. 2013. *Development of Flexible Link Slabs using Ductile Fiber Reinforced Concrete*. PhD Thesis, Technical University of Denmark, Lyngby, Denmark.
- Li, V. C., E. H., Yang, and M. Li. 2008. *Field Demonstration of Durable Link Slabs for Jointless Bridge Decks Based on Strain-Hardening Cementitious Composites—Phase 3: Shrinkage Control*. Research Report RC-1506. Michigan Department of Transportation.
- Li, V.C., and M. D. Lepech. 2009. *Application of ECC for Bridge Deck Link Slabs*. *Materials and Structures*, Vol. 42, Issue 9, pp. 1185-1195.

- Li, V. C., M. D., Lepech, and M. Li. 2005. *Field Demonstration of Durable Link Slabs for Jointless Bridge Decks Based on Strain-Hardening Cementitious Composites*. Research Report RC-1471. Michigan Department of Transportation.
- Li, V. C. 2008. *Engineered Cementitious Composites (ECC) Material, Structural, and Durability Performance*, University of Michigan, Ann Arbor, MI.
- Mohod, M. V. 2015. *Performance of polypropylene fibre reinforced concrete*. Journal of Mechanical and Civil Engineering, Vol. 12, No. 1, pp. 28-36.
- Mohammadi Mohaghegh, A. 2016. *Use of Macro Basalt Fibre Concrete for Marine Applications*. Doctoral Dissertation, KTH Royal Institute of Technology.
- Okeil, A. M., and A. ElSafty. 2005. *Partial continuity in bridge girders with jointless decks*. Practice Periodical on Structural Design and Construction, Vol. 10, No. 4, pp. 229-238.
- Ozyildirim, C., E. Khakimova, H. Nair, and G.M. Moruza. 2016. *High-Performance Fiber-Reinforced Concrete in Closure Pours over Piers*. In Transportation Research Board 95th Annual Meeting (No. 16-3669).
- Patnaik, A., S. Bajaj, J. Lewis, J. Payer, & R. Liang. 2013. *Retardation of strength degradation of reinforced concrete due to steel bar corrosion with fiber additions*. DOD Virtual Corrosion Conference, pp. 16-17.
- Patnaik, A., L. Miller, & P. C. 2014. *Standal. Fiber reinforced concrete made from Basalt FRP Minibar*. Concrete Innovation Conference, pp. 11-13.
- Patnaik, A. 2013. *MiniBar Reinforced Concrete (MRC)*. Report RFT-AP-MB-R03, University of Akron, Akron, OH.
- Roque, R., N. Kim, B. Kim, & G. Lopp. 2009. *Durability of fiber-reinforced concrete in Florida environments*, University of Florida, Tallahassee FL.
- Richardson, D. R. 1989. *Simplified Design Procedures for the Removal of Expansion Joints from Bridges Using Partial Debonded Continuous Decks*. MSCE Thesis, North Carolina State University, Raleigh, NC.
- Ryes, J., and I. N. Robertson. 2011. *Precast Link Slabs for Jointless Bridge Decks*. Research Report UHM-CEE-11-09. FHWA, U.S. Department of Transportation.
- Samani, G. S. 2013. *Structural Performance of Link Slabs Subjected to Monotonic and Fatigue Loading Incorporating Engineered Cementitious Composites*. MSCE Thesis, Ryerson University, Toronto, Canada.
- Shafiq, N., T. Ayub, & S. U. Khan. 2016. *Investigating the performance of PVA and Basalt fibre reinforced beams subjected to flexural action*. Composite Structures, Vol. 153, pp. 30-41.
- Studinka, J. B. 1989. *Asbestos substitution in the fibre cement industry*. International Journal of Cement Composites and Lightweight Concrete, Vol. 11, No. 2, pp. 73-78.
- Thomas, J., & A. Ramaswamy. 2007. *Mechanical properties of steel fiber-reinforced concrete*. Journal of Materials in Civil Engineering, Vol. 19, No. 5, pp. 385-392.
- Taylor, P., X. Wang, and X. Wang. 2015. *Concrete Pavement Mixture Design and Analysis (MDA): Development and Evaluation of Vibrating Kelly Ball Test (VKelly Test) for the Workability of Concrete*. InTrans Project Reports.

- Ulku, E., U. Attanayake, and H. Aktan. 2009. *Jointless Bridge Deck with Link Slabs: Design for Durability*. In Transportation Research Record: Journal of the Transportation Research Board, No. 2131, Transportation Research Board of the National Academies, Washington D.C., pp. 68-78.
- Wu, G., X. Wang, Z. Wu, Z. Dong, & G. Zhang. 2015. *Durability of basalt fibers and composites in corrosive environments*. Journal of Composite Materials, Vol. 49, No. 7, pp. 873-887.
- Wing, K. M., and M. J. Kowalsky. 2005. *Behavior, Analysis, and Design of an Instrumented Link Slab Bridge*. Journal of Bridge Engineering, Vol. 10, No. 3, pp. 331-344.
- Zheng, Z., & D. Feldman. 1995. *Synthetic fibre-reinforced concrete*. Progress in Polymer Science, Vol. 20, No. 2, pp. 185-210.
- Yan, F., & Lin, Z. 2017. *Bond durability assessment and long-term degradation prediction for GFRP bars to fiber-reinforced concrete under saline solutions*. Composite Structures, 161, 393-406.
- Zuk, W. 1981. *Jointless Bridges*. Research Report No. FHWA/VA-81-48. Virginia Highway and Transportation Research Council.